HHS Public Access

Author manuscript

Neuron. Author manuscript; available in PMC 2022 October 20.

Published in final edited form as:

Neuron. 2021 October 20; 109(20): 3252–3267.e6. doi:10.1016/j.neuron.2021.07.028.

A hidden threshold in motor neuron gene networks revealed by modulation of miR-218 dose

Neal D. Amin[1,2,*], **Gokhan Senturk**[1], **Giancarlo Costaguta**[1], **Shawn Driscoll**[1], **Brendan O'Leary**[1], **Dario Bonanomi**[1,3], **Samuel L. Pfaff**[1,†,*]

[1]Gene Expression Laboratory, Salk Institute for Biological Studies, 10010 North Torrey Pines, La Jolla, CA 92037, USA

[2]Present address: Department of Psychiatry and Behavioral Sciences, Stanford University, Stanford, CA 94305, USA

[3]Present address: San Raffaele Scientific Institute, Division of Neuroscience, via Olgettina 60, 20132 Milan, Italy

Summary

Disruption of homeostatic miRNA expression levels is known to cause human neuropathology. However, the gene regulatory and phenotypic effects of altering a miRNA's *in vivo* abundance (rather than its binary gain or loss) is not well understood. By genetic combination, we generated an allelic series of mice expressing varying levels of miR-218, a motor neuron-selective gene regulator associated with motor neuron disease. Titration of miR-218 cellular dose unexpectedly revealed complex, non-ratiometric target mRNA dose responses and distinct gene network outputs. A non-linearly responsive regulon exhibited a steep miR-218 dose-dependent threshold in repression, that when crossed, resulted in severe motor neuron synaptic failure and death. This work demonstrates that a miRNA can govern distinct gene network outputs at different expression levels and that miRNA-dependent phenotypes emerge at particular dose ranges due to hidden regulatory inflection points of their underlying gene networks.

[*]**Corresponding authors contact:** Sam Pfaff, pfaff@salk.edu, Neal Amin, nealamin@stanford.edu.

AUTHOR CONTRIBUTIONS

N.D.A. and S.L.P. designed the study and wrote the manuscript. N.D.A. carried out the experiments with assistance from B.O. and G.C. D.B. generated sensory neuron RNA sequencing data. G.S. performed RNAscope experiments. N.D.A., S.L.P. and D.B. revised the manuscript. N.D.A. analyzed bulk RNA sequencing data and S.P.D. and N.D.A. analyzed single cell sequencing data.

[†]Lead contact

DECLARATION OF INTERESTS

The authors note a related US patent related to motor neuron specific expression vectors (US patent US Patent 10,729,790)

INCLUSION AND DIVERSITY

We worked to ensure sex balance in the selection of non-human subjects. While citing references scientifically relevant for this work, we also actively worked to promote gender balance in our reference list.

CONTACT FOR REAGENT AND RESOURCE SHARING

Further information and requests for resources and reagents should be directed to and will be fulfilled by the Lead Contact, Samuel Pfaff (pfaff@salk.edu).

SUPPLEMENTAL INFORMATION

Supplemental information can be found with this article.

Graphical Abstract

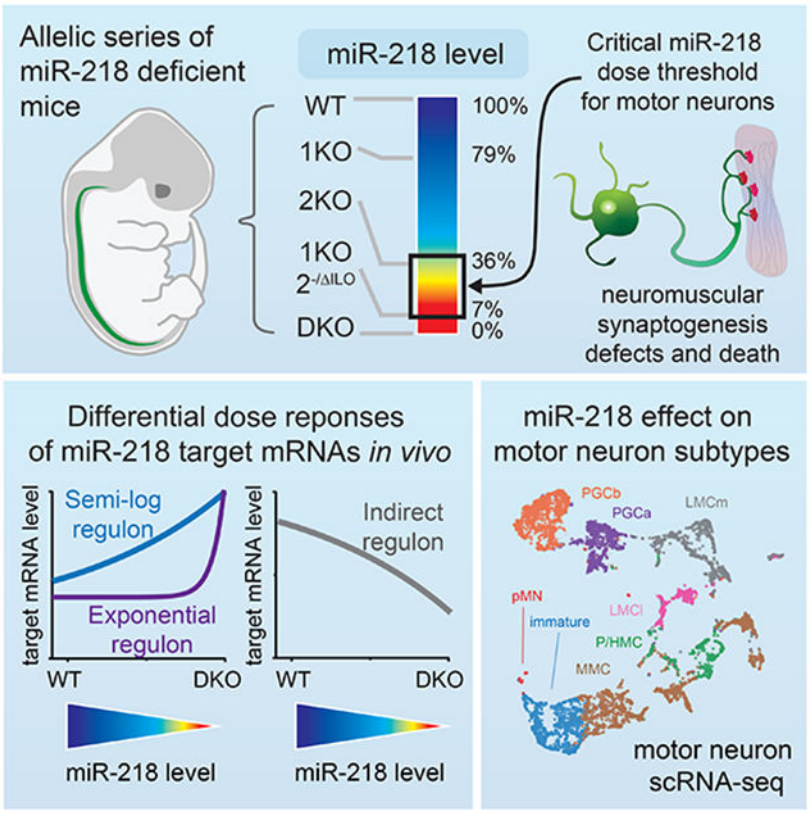

In Brief

By genetically titrating the levels of the ALS-associated miR-218 in mice, Amin et al. reveals an *in vivo* inflection point in target mRNA repression that underlies a phenotypic threshold for neuromotor defects and survival.

Introduction

Two-state, wild type-versus-knockout experimental frameworks have been critical to establish broad gene regulatory and biological effects of many essential miRNAs in the nervous system (Bartel, 2018; Park et al., 2010). However, reductions in miRNA expression, rather than complete loss, are associated with neuropsychiatric disorders (Butti and Patten, 2018; Geaghan and Cairns, 2015; Kamal et al., 2015; Magri et al., 2018; Paul et al., 2018; Sadlon et al., 2019). A variety of factors can perturb homeostatic miRNA levels and lead to gene network dysregulation and pathology, including inherited genetic variants (Cheng et al., 2018), cancer (Palanichamy and Rao, 2014), proteinopathies (Emde et al., 2015), and environmental triggers such as aging (Inukai et al., 2018). In a well-studied case, inherited haploinsufficiency of a miRNA in humans has been shown to cause progressive sensory neurodegeneration and hearing loss (Mencia et al., 2009; Solda et al., 2012). Despite the relevance of intermediate miRNA levels to nervous system disease states, the effect

of modulating *in vivo* miRNA cellular dose on target mRNA selection, gene network regulation, and neuronal phenotypes has not been investigated.

We sought to systematically investigate the effects of varying the *in vivo* expression level of miR-218, the most abundant and highly enriched miRNA in developing and mature motor neurons (Amin et al., 2015; Shu et al., 2019; Thiebes et al., 2015). We previously showed that complete loss of miR-218 results in a breakdown of neuromuscular synaptogenesis, motor neuron loss, and complete paralysis (Amin et al., 2015). Rare human miR-218 gene variants have since been identified in ALS patients that may perturb its biogenesis, thus contributing to the development of neuropathology (Reichenstein et al., 2019). Furthermore, mutations in proteins that affect miRNA biogenesis such as SMN, FUS, HNRNPA1, and TDP43 are known causes of motor neuron diseases, suggesting miRNA dysregulation may be a shared feature of these degenerative diseases (Buratti et al., 2010; Nussbacher et al., 2019; Volonte et al., 2015). Interestingly, only miR-218 was consistently found to have significantly reduced expression levels across multiple miRNA profiling studies of spinal cords from ALS patient cohorts (Figure 1A-C and Figure S1A-C) (Butovsky et al., 2015; Campos-Melo et al., 2013; Emde et al., 2015; Figueroa-Romero et al., 2016; Reichenstein et al., 2019). miR-218's specific and abundant expression in motor neurons, critical importance for mammalian neuromotor function, and hypothesized roles in motor neuron disease pathogenesis motivated us to investigate its dose-dependent regulatory and phenotypic effects.

Here, we systematically altered *in vivo* miR-218 expression levels in motor neurons by generating an allelic series of mice carrying combinations of up to three independent genetic mutations affecting miR-218 production. Modulation of miR-218 levels revealed non-ratiometric regulatory outputs on multiple miR-218 regulons – sets of genes exhibiting similar miR-218 dose-dependent regulatory effects. Threshold-like phenotypic outcomes were strongly associated with an underlying steep inflection point in the de-repression of a non-linearly dose-responsive regulon distinguished by 3'UTR features. We further investigate downstream gene network effects upon a coherent subset of indirect miR-218 targets and identify miR-218 dose-dependent effects upon motor subpopulations using single cell RNA sequencing. These studies reveal that gene regulation and emergence of lethal phenotypes are heavily influenced by relative miRNA expression levels due to previously unappreciated dynamic and varied dose-responses of individual target mRNAs.

Results

Reducing motor neuron-specific transcription of pri-miR-218-2

Mature miR-218 is generated from two alleles, miR-218-1 and miR-218-2, embedded within the *Slit2* and *Slit3* genes, respectively (Figure 2A). Transcription of canonical *Slit2* and *Slit3* mRNAs begins at exon 1 (Brose et al., 1999), whereas primary miR-218 transcripts (pri-miR-218-1 and pri-miR-218-2) initiate transcription upstream of exon 6 in mouse and human motor neurons (Figure S2A) (Amin et al., 2015). Highly-conserved motor neuron transcription factor binding sites were promising candidates as cis-regulatory elements due to their proximity to pri-miR-218-2's transcription start site (Figure 2B) (Rhee et al., 2016). We screened the influence of these putative cis-elements on pri-miR-218-2 transcripts

(embedded within the *Slit3* gene) in motor neurons by inducing a series of multiplexed deletions using CRISPR-Cas9 in mouse embryonic stem cells (mESCs) carrying the transgenic motor neuron reporter *Hb9::gfp* (Figure S2B and S2C, Table S1). mESCs were differentiated over 6 days into GFP+ motor neurons, which were subsequently isolated by fluorescent activated cell sorting (FACS) for RNA sequencing. A microdeletion eliminating a single binding site for Isl1, Lhx3, and Onecut1 abolished expression of pri-miR-218-2 in motor neurons and did not affect *Slit3* mRNA generated from the canonical exon 1 promoter (Figure S2D-G). We cloned a DNA fragment containing these cis-elements into a promoter-less vector to determine whether this compact 908bp genomic unit was sufficient to drive specific motor neuron expression (Figure S2H). In both the chick neural tube and transgenic mice, reporter expression was abundant and restricted to motor neurons (Figure S2I and S2J). While miR-218 is encoded within the Slit3 gene body, motor neuron-specific and independently active cis-regulatory elements decouple pri-miR-218-2 and Slit3 transcription. Thus, we show that miR-218 is a rare example of a miRNA located within an intron of a protein-coding gene that is independently transcribed (Ramalingam et al., 2014).

Next, we used these *in vitro* findings to design a mutation that would reduce, but not completely eliminate motor neuron expression of mouse miR-218 *in vivo*. By oocyte microinjection of Cas9 mRNA and gRNAs, we generated a 264bp deletion of the Isl1/Lhx3/Oc1 binding sites (named 218-2$^{\Delta ILO}$) located directly upstream of the start site for pri-miR-218-2's transcription (Figure 2B and 2C). As desired, this smaller 218-2$^{\Delta ILO}$ mutation reduced but did not eliminate *in vivo* transcription of pri-miR-218-2 in motor neurons (Figure 2D, Figure S2K and S2L). This led to de-repression of miR-218 target genes in FACS-isolated 218-2$^{\Delta ILO/\Delta ILO}$ motor neurons compared to wild type (WT) controls ($p=3.8 \times 10^{-25}$, chi-square test, Figure S2M). Thus, our *in vitro* mutation screen in mESC-derived motor neurons informed the design of a mouse allele that reduces miR-218 expression *in vivo* by partially decreasing pri-miR-218-2 transcription from its motor neuron-specific promoter.

Variation in phenotypic severity in an allelic series of miR-218 deficient mice

To systematically investigate how miR-218 levels affect motor phenotypes, we generated an allelic series of mice with graded expression levels of *in vivo* miR-218. This was achieved by combining previously generated mouse knockout mutations that completely eliminate pre-miR-218-1 and pre-miR-218-2 genomic sequences (Amin et al., 2015) along with the newly generated 218-2$^{\Delta ILO}$ mutation that reduces transcription.

Examination of mice carrying homozygous null mutations in pre-miR-218-2 (2KO) revealed many neonates died within 3 days after birth (Figure 2E, Figure S2N) and survivors were typically runted (Figure S2O). The incompletely penetrant phenotype of 2KO mice suggested the level of miR-218 expressed in these mutants was near the critical threshold for motor function to support life. In contrast, mice with homozygous null mutations in pre-miR-218-1 (1KO) were born in Mendelian ratios and appeared overtly normal (Figure S2P).

As previously described, miR-218-1$^{-/-}$;miR-218-2$^{-/-}$ double knockout (DKO) mice entirely lack miR-218 expression and are not viable at birth, displaying kyphosis, neuromuscular

synaptic defects, and motor neuron degeneration (Amin et al., 2015). Interestingly, we find that miR-218-1$^{-/-}$;−218-2$^{-/+}$ mice that express miR-218 from a single genomic pri-miR-218-2 allele were viable and had normal motor function (Figure S2Q), indicating that the miR-218 dose threshold for viability was in between the miR-218-1$^{-/-}$;−218-2$^{-/+}$ and DKO genotypes. We explored the effect of finely titrating miR-218 levels between these two genetic states by replacing the remaining functional pri-miR-218-2 allele with the transcriptionally diminished 218-2$^{\Delta ILO}$ allele in compound heterozygous miR-218-1$^{-/-}$;218-2$^{-/\Delta ILO}$ mice (1KO;2$^{-/\Delta ILO}$). Immunostaining of 1KO;2$^{-/\Delta ILO}$ limb muscle tissue at E18 revealed immunohistological defects in neuromuscular synaptogenesis (Figure 2F,G). 1KO;2$^{-/\Delta ILO}$ mice died at birth (or after E18 when delivered by cesarean section) from apparent lack of respiration (Figure 2H and S2Q). This indicated that the diminished transcriptional activity of the 218-2$^{\Delta ILO}$ allele alone cannot generate sufficient levels of miR-218 to support neuromuscular function and mouse survival.

To quantitatively measure miR-218 expression levels associated with *in vivo* motor phenotypes, we FACS-purified *Hb9::gfp*+ E12 motor neurons from each of five genotypes in biological triplicates from independent mouse embryos for Taqman miRNA qPCR (Figure 3A). Motor neuron expression of miR-218 spanned a wide range across genotypes (Figure 3B) and inversely correlated with phenotypic severity (Figure 3C). Based on the association between genotype, miR-218 level, and phenotype, we identify a critical miR-218 dose-threshold point between 7-36% of wild type levels required to support motor neuron function and post-natal mammalian viability.

miR-218 targets have varied dose-response characteristics

We next examined the specific gene regulatory changes that underlie miR-218 dose-dependent motor neuron phenotypes in a dose-response gene network analysis. We performed RNA sequencing on FACS-purified E12 motor neurons across 5 genotypes: WT, 1KO, 2KO, 1KO;2$^{-/\Delta ILO}$, and DKO (Figure 3A, S3A and S3B, Table S2). The hypergeometric 3'UTR motif enrichment tool Sylamer was used to assess the detection quality of miRNA-mediated effects in our motor neuron-specific transcriptome data (van Dongen et al., 2008). We observed specific and statistically significant de-repression of mRNAs with canonical miR-218 binding sites in their 3'UTRs (Figure S3C). 316 target mRNAs were significantly de-repressed in DKO motor neurons and possessed high confidence predicted miR-218 binding sites (92.2%; p=6.8x10^{-55}, Chi-squared test) (Agarwal et al., 2015) (Figure 3D, S3D and S3E). Across the allelic series of motor neuron genotypes, graded reductions in miR-218 expression resulted in statistically significant stepwise increases in the expression of the population of 316 target mRNAs (Figure 3E). These results clearly demonstrate that miRNA dose precisely modulates the overall repression magnitude of endogenous target mRNAs *in vivo*.

Our null hypothesis was that each individual target mRNA would exhibit a uniform, inversely proportional relationship between miR-218 dose and mRNAs expression. However, hierarchical clustering of gene expression showed that the relationship between miRNA dose and target mRNA de-repression varied considerably across individual mRNAs (Figure 3F). Furthermore, different genotypes displayed non-overlapping sets

of de-repressed genes (Figure S3F). These findings indicated that, in contrast to our null hypothesis, miRNA-dose responses are not uniform across mRNA targets. We next examined if relative decreases in miR-218 expression cause a fixed percentage increase in the levels of any target mRNAs, which would be reflected by a semi-log (i.e. log-linear) dose relationship. A subset of mRNA targets that we term the miR-218 semi-log regulon was well modelled with a semi-log regression (Figure 3G, 3H, and S3G). In contrast, a semi-log regression poorly fit the dose-response curves of other mRNA targets, suggesting that many miR-218 targets have more complex dose-response relationships that had not been previously anticipated.

A hidden inflection point in miR-218-mediated repression of an exponential regulon

Surprisingly, we observed that the gene expression of a distinct regulon of miR-218 target mRNAs was not affected by large decreases in miR-218 levels between WT to 1KO to 2KO motor neuron genotypes (Figure 3I and 3J). Remarkably, when levels further decreased beyond this miR-218 dose inflection point, these targets became highly dose-responsive and steeply de-repressed in 1KO;$2^{-/\Delta ILO}$ and DKO mutants. In contrast to the semi-log regulon in which dose-responses (i.e. rates of change) are static over a wide range of miR-218 doses, the dose-sensitivity of this set of mRNAs dynamically decreases relative to increasing levels of miR-218. An additional key feature of this set of genes was that their miR-218-mediated repression reaches a saturation point after which they were unexpectedly no longer repressed any further by greater levels of miR-218 expression. The dose-response curves of these target mRNAs strongly fit an exponential rather than a semi-log regression (extra sum of squares F test, Figure 3I and 3J). The inflection dose-point for the de-repression of this exponential regulon correlates with the miR-218 dose at which we observed neuromuscular synaptogenesis failure and neonatal death, suggesting a close relationship between the dysregulation of the exponential regulon and the emergence of *in vivo* phenotypic thresholds. Thus, decreases in miR-218 expression cause motor neuron dysfunction only when a hidden threshold of repression of a particular regulon is crossed.

Dose responsivity is associated with 3'UTR features

This dose-response network analysis suggests that the emergence of miRNA-mediated biological phenotypes is strongly related to subnetworks of target genes with non-linear dose response characteristics. To examine how endogenous variation in miRNA-mediated dose response characteristics might arise, we explored a number of miRNA targeting and RNA structural features that could influence whether a target mRNA has either semi-log or exponential miR-218 dose responses. Despite their wide differences in miRNA dose-response dynamics, we find that semi-log and exponential regulons did not differ in their overall magnitude of repression between WT and DKO motor neurons (Figure 4A). Bioinformatic models of miRNA targeting have incorporated biological and computational attributes from experimentally validated datasets and can predict miRNA targeting strength (Agarwal et al., 2015). Nevertheless, the semi-log and exponential regulons did not differ in previously reported predicted miRNA targeting efficacy (Figure 4B). These findings indicate that *in vivo* miRNA dose-response characteristics are not simply reflective of repression strength and cannot be accounted for by existing models of miRNA-targeting.

We hypothesized that target mRNA's 3'UTRs might influence miRNA dose-responsiveness since they are a regulatory hub for miRNA targeting, mRNA trafficking, and turnover. Though alternative splicing and polyadenylation can alter the presence or absence of particular 3'UTR miRNA binding sites, semi-log and exponential regulons did not vary by 3'UTR isoform profiles (data not shown). However, we found that 3'UTRs were significantly longer in the semi-log versus exponential regulons, while, in contrast, 5'UTR length did not differ (Figure 4C). We also found more miR-218 response elements (MREs) per 3'UTR in the semi-log regulon (Figure 4D), though the overall density of MREs per kilobase of 3'UTR was not different (data not shown).

We did not find that MREs with a specific size, type of seed match, or conservation had a stronger association with either regulon (Figure S4A-C), indicating that the number of MREs rather than variant class influences dose responsiveness. We also find that the semi-log regulon has lower cellular abundance than the exponential regulon, consistent with previous reports that mRNAs with long 3'UTRs are generally associated with lower absolute expression levels (Figure 4E) (Matoulkova et al., 2012). 3'UTRs influence mRNA trafficking to subcellular compartments, which in turn might influence dose response parameters in highly polarized cell types like motor neurons. Indeed, genes within the exponential regulon exhibit greater enrichment in motor neuron axonal versus somatic compartments, indicating that mRNA localization may impact miRNA dose-responsiveness (Figure 4F) (Nijssen et al., 2018).

Are the semilog and exponential regulons discrete entities or do miRNA targets exist along a dose-responsive continuum? To address this question, we used a continuous variable reflecting dose-responsiveness of individual miR-218 targets based upon the miRNA dose at which 50% repression is achieved, termed ½ max repression (Figure S4D). We observe a non-normal distribution of ½ max repression values and a specific enrichment in low values that correspond to the exponential regulon (Figure S4E-G). Since continuous variables can provide greater statistical power than categorical variables, we also used ½ max repression values to examine correlations of 3'UTR features with exponential and semi-log regulons. This complementary statistical analysis confirms the association of miR-218 target dose responsiveness with the number of miR-218 MREs, transcript abundance, soma versus axonal enrichment, and 3'UTR length (Figure S4H-J). These results demonstrate that dose responsiveness is not normally distributed, revealing semi-log and exponential regulons are distinct.

To examine potential functional consequences of dose responsive regulons, we examined gene ontology associations. We found that the exponential regulon is enriched in synaptic vesicle priming and axon development categories, consistent with our observed *in vivo* phenotypic effects upon neuromuscular synaptogenesis (Figure 4G). Differences in gene ontology enrichments between semi-log and exponential regulons suggest that functionally distinct sets of target mRNAs can be controlled by altering the cellular dose of a single miRNA. In summary, we find that 3'UTR features are associated with differences in miRNA dose responses of individual mRNA targets (Figure 4H), suggesting a new role for how mRNA 3'UTRs can set miRNA dose responsiveness.

Indirect activation of a peripheral neuronal gene signature by miR-218

The repressive effects of miRNAs are thought to propagate through cellular gene networks to cause downstream (indirect) effects on gene expression, which may in turn affect biological phenotypes (Carroll et al., 2013; McGeary et al., 2019; Nam et al., 2014). However, the magnitude and importance of potential miRNA-mediated indirect effects in relation to direct repressive effects are unclear and their potential relevance to the regulation of neuronal gene networks is not well understood (Nam et al., 2014; Rajman and Schratt, 2017).

We used our transcriptome data to investigate transcripts that were highly affected by miR-218 to identify and characterize the strongest indirect effects. The majority of genes that are de-repressed by 2-fold have miR-218 MREs and are thus likely to be primary miR-218 targets (Figure S5A). In contrast, 64 genes de-activated by 2-fold lacked 3'UTR miR-218 binding sites indicating they are indirectly activated by miR-218 (Figure 5A,B). We term this cohort of 64 high confidence and highly affected genes the indirect regulon. Inverse to direct targets, the expression of the indirect regulon incrementally decreases as levels of miR-218 decline across the allelic series, demonstrating downstream miRNA-mediated effects are also dose sensitive (Figure 5C). The dose-response characteristics of the individual genes comprising the indirect regulon varied, suggesting complex dynamics of intracellular gene networks that might buffer or potentiate the primary direct target effects (Figure S5B-F). Interestingly, primary and downstream target mRNA changes were similar in absolute magnitude (up to ~4-fold) and the indirect regulon was enriched for vesicular and synaptic functions in gene ontology categories that relate to phenotypes observed in miR-218 DKO mutant motor neurons (Figure 5D). These findings suggest that indirect effects might have important and potentially distinct contributions to motor neuron function compared to mRNAs directly repressed by miR-218.

The spatial expression patterns of miRNA target genes can provide unique insights into their regulatory roles in shaping neuronal function (Shkumatava et al., 2009). In contrast to direct miR-218 targets which are pan-neuronally expressed (Amin et al., 2015), we unexpectedly found a remarkably strong and specific association of the indirect regulon with the dorsal root ganglia (DRG) in the Pattern Gene Database (Figure 5D), although miR-218 is not expressed in the DRG (Amin et al., 2015). Thus, we were surprised that the indirect gene targets were enriched in both motor neurons and DRG neurons, a distinct peripheral nervous system (PNS) neuronal population derived from neural crest cells. Gene networks shared by these two neuronal types had not been previously identified. To explore this association further, we referenced the Allen Brain Atlas to examine the *in situ* spatial expression of indirect regulon RNAs in the spinal cord and surrounding tissues (Figure 5E and S5G, Table S3). We confirmed the specific, shared expression pattern of indirect regulon genes in both DRG and motor neurons. In contrast, indirect regulon genes were largely absent from spinal interneurons, glia, and other surrounding cell types (Figure 5E and S5G). We next used RNAscope to examine *in situ* RNA expression of Prph (the most highly expressed indirect regulon mRNA) (Figure 5A) in motor and DRG neurons in WT and DKO tissues. We found that Prph expression is selectively reduced in DKO motor neurons while unaffected in DKO DRG neurons (Figure 5F). These results demonstrate that miR-218 indirectly activates this

regulon in motor neurons whereas DRG neurons utilize a distinct gene regulatory pathway to activate this gene set.

To accurately quantify the indirect regulon's spatial enrichment pattern and the transcriptomic differences between these neuronal populations, we profiled transcriptomes from microdissected and FACS-isolated DRG cells from Wnt1:Cre; Rosa:LSL:tdTomato mouse embryos (Figure 5G) to compare with our motor neuron data and previously obtained age-matched transcriptomes from V1, V2a and V3 ventral spinal interneuron populations (Amin et al., 2015). Using principal components analysis (PCA), we found that the transcriptional identities of spinal interneurons clustered tightly together, while spinal motor neurons were located between CNS-derived interneurons and PNS-derived DRG neurons along PC2 (Figure 5H). This may reflect motor neuron's dual CNS and PNS identities, as spinal motor neuron cell bodies are located in the CNS while their axons travel within specialized PNS nerve bundles together with DRG sensory fibers (Suter and Jaworski, 2019). We compared enrichment of individual genes across the three populations in a fold-change versus fold-change plot (Figure 5I). Isl1 and Isl2 served as positive controls as they are two known transcription factor markers of both motor and DRG neurons that are absent from ventral interneurons. Indeed, both Isl1 and Isl2 were the most highly co-enriched mRNAs in motor and DRG transcriptomes (Figure 5I, Table S4). Remarkably the next two most motor neuron and DRG-enriched genes are annexin A2 (Anxa2) and peripherin (Prph) – both of which are miR-218 indirect regulon mRNAs. In total, 57 of 64 mRNAs in the indirect regulon were expressed higher in motor and DRG neurons versus CNS interneurons (89%, p=3.6x10^-20; chi squared test).

These analyses identified a surprising and unanticipated relationship between miR-218's downstream indirect effects and a set of PNS-associated genes that are also expressed in CNS-derived motor neurons, despite their distinct developmental origins and neuronal functions from DRG neurons that lack miR-218. This novel gene network may contribute to the unique peripheral-specific functions of CNS-derived motor neurons. These findings demonstrate that a miRNA's indirect effects can represent coherent gene networks identified by co-enrichment in otherwise distinct cell populations.

miR-218 is not required for motor neuron subtype specification

Motor neurons are diverse and have been categorized into subtypes that express unique combinations of transcription factors, migrate to particular columnar locations within the spinal cord, and project peripheral axons to specific muscle and visceral targets (Figure 6A) (Alaynick et al., 2011; Philippidou and Dasen, 2013; Shirasaki and Pfaff, 2002). Previous transcriptomic profiling efforts examining miR-218-mediated effects have treated motor neurons as a single population (Amin et al., 2015; Thiebes et al., 2015). However, miR-218 may impact motor neuron subtype acquisition or have context-specific effects within a motor subpopulation. To investigate motor neuron diversity in the presence and absence of miR-218, we sorted *Hb9::gfp*+ motor neurons from WT and DKO mouse embryos in duplicate and performed droplet-based single cell RNA sequencing (Figure 6B and S6A). Choline acetyltransferase (ChAT)-expressing motor neurons constituted the majority of the collected cells with a minority of contaminating ChAT- spinal interneurons (Figure S6B).

Using a guided approach based upon the known expression of subtype-specific transcription factors and rostro-caudal Hox code marker genes (Alaynick et al., 2011; Jung et al., 2014), we identified motor neurons belonging to axial, lateral, and preganglionic motor column identities spanning cervical to lumbar spinal cord regions (Figure 6C-E, S6C and S6D). We unexpectedly found that preganglionic (PGC) motor neurons controlling visceral functions segregated into two spatially distinct UMAP clusters that we term PGCa and PGCb. This division of visceral motor neurons was marked by the presence or absence of FoxP1 and Isl1 and were additionally distinguished by neuropeptide expression (e.g. vasopressin and CART prepropeptide). Previously identified divisions within the axial (i.e. MMC and P/HMC) and lateral motor columns (i.e. LMCl and LMCm) correspond to differences in axonal projection patterns and muscle targets. Likewise, the segregation of PGC motor neurons into two divisions indicates that PGCa and PGCb cells may have distinct visceral targets and potentially divergent functions (Figure S6E). We also found that immature motor neurons are most similar to MMC axial motor neurons, which are among the evolutionarily-oldest motor neurons found in non-limbed vertebrates (Figure 6C) (Shirasaki and Pfaff, 2002). This is consistent with the prediction that immature motor neurons with MMC-like characteristics served as the ground state for further motor neuron diversification over evolutionary time.

We examined if loss of miR-218 affected motor subtype cell fate acquisition. Pseudo-time cellular trajectory analysis provided a detailed view of the sequential activation and deactivation of transcription factors during the transition of motor neuron progenitors (pMN) into a post-mitotic mature state (Figure S6F). WT and DKO motor neurons did not appreciably segregate in cellular trajectory space or in sequential gene programs (Figure 6F). Individual motor neuron subtypes contained both WT and DKO motor neurons and the relative proportions of motor subtypes was not significantly altered, indicating that miR-218 does not greatly impact motor neuron subtype specification (Figure 6G and 6H). Unlike previously identified transcription factor-mediated gene networks, our analysis indicates that miR-218-mediated repression is not needed for motor neuron cell fate or subtype acquisition. Thus, miR-218 is unlike other well studied neuronal-enriched miRNAs such as miR-9 and miR-124 that have well elucidated roles in the regulation of neurogenesis (Makeyev et al., 2007; Yoo et al., 2011).

Identification of miR-218-mediated effects from scRNA sequencing

scRNA sequencing data is typically used to evaluate cellular diversity but has the potential to reveal gene expression changes within particular cell types that would otherwise be missed by signal dilution from bulk RNA sequencing of whole populations. However, scRNA sequencing analysis is inherently limited compared with bulk RNAseq by transcriptome coverage, gene dropouts, and noise. Our strategy to overcome these issues was to generate pseudo-bulk transcriptomes from *in silico* collections of single cells, starting with WT and DKO motor neurons and the smaller proportion of collected interneurons. Sylamer was used to detect the enrichment of 3'UTR motifs among genes expressed higher in DKO versus WT pseudo-bulk motor neurons. As with bulk RNAseq analysis (Figure S3C), miR-218's seed sequence match was the only enriched 3'UTR motif detected, reflecting the specific de-repression of mRNAs carrying miR-218 binding sites (Figure 7A). Serving as an internal negative control, WT and DKO pseudo-bulk interneurons did not have a specific

3’UTR motif enrichment, reflecting the lack of miR-218 expression and repressive effects in interneurons (Figure 7B). Examination of 3’UTR motif enrichment in WT pseudo-bulk interneurons versus WT pseudo-bulk motor neurons identified the specific enrichment of miR-218’s seed sequence (Figure 7C). This enrichment was eliminated in DKO pseudo-bulk motor neurons (Figure 7D), confirming our previous finding that miR-218 independently represses a pan-neuronal cohort of genes specifically in motor neurons (Amin et al., 2015). Using differential expression testing on pseudo-bulk populations, we additionally confirmed de-repression and de-activation of previously identified direct and indirect miR-218 target genes, respectively, in pseudo-bulk DKO motor neurons but not DKO interneurons (Figure S7A-D). In summary, we establish that pseudo-bulk differential expression analysis of WT and DKO scRNAseq data is effective in detecting highly significant and cell type-specific miR-218-mediated effects in motor neurons.

miR-218-mediated effects vary by magnitude, but not character, across motor neuron subtypes

We examined the effects of miR-218 upon transcriptomes of individual motor neuron subtypes by first generating pseudo-bulk transcriptomes of motor neurons from the same motor column and genotype. Hierarchical clustering identified that pseudo-bulk replicates clustered together, reflecting biological reproducibility (Figure 7E, Table S5,6). We found that the major division of pseudo-bulk populations is between somatic (MMC, P/HMC, LMCm, and LMCl) and visceral (PGCa and PGCb) motor neurons. PCA analysis demonstrated that somatic and visceral pseudo-bulk motor neurons segregate along PC1 (21.0% of variance; Figure 7F and S7E). This transcriptional distinction between somatic and visceral motor neurons likely reflects important functional and connectivity differences associated with autonomic and voluntary motor control. The next major hierarchical clustering division was between WT and DKO genotypes and PCA analysis revealed that PC2 (17.8% of variance) distinguishes WT from DKO motor neurons (Figure 7E and 7F). The similar level of variance captured by PC1 and PC2 indicates that miR-218-mediated transcriptomic changes are comparable in magnitude to those that distinguish somatic and visceral motor neuron subtypes.

Since PC2 separated WT and DKO motor neurons regardless of subtype, we considered if the effects of miR-218 within motor neuron subtypes might be highly similar. To investigate the effect of miR-218 upon individual subtypes, we performed differential expression testing of mRNAs with strong predicted miR-218 binding sites within each pseudo-bulk motor neuron subtype (Figure 7G and S7F). We identified targets not previously detected by bulk RNA sequencing which may represent a minority of motor neuron subtype-specific miR-218 targets (Figure S7G-H). Nevertheless, we generally found targets were expressed across subtypes and we found high correlation between the fold changes of individual direct and indirect miR-218 target genes by subtype (Figure 7H and S7I). Next, we compared the magnitude of miR-218-mediated repression of direct targets with the magnitude of activation of indirect targets by motor subtype. We found a strong linear correlation between direct and indirect effects (Figure 7I). Yet, we observed a wide range of effect magnitudes among motor neuron subpopulations. Notably, PGCb motor neurons exhibit ~35% less miR-218-mediated effects on both direct and indirect targets compared with MMC motor neurons.

Thus, motor column subtypes display different magnitudes of miR-218-mediated effects on both direct and indirect targets.

We hypothesized that differences in effect magnitude could be due to inherent differences in levels of miR-218 expression in motor columns. We examined the relationship between the levels of miR-218's primary transcripts (pri-miR-218-1 and pri-miR-218-2) and the magnitude of repression of miR-218 regulons by subtype (Figure 7J, 7K, S7J and S7K). Reads that mapped to the Slit2/3 gene body were annotated as pri-miR-218-1/2 as we previously found that the majority RNA sequencing reads from motor neurons map to the latter (Amin et al., 2015). In motor neuron subtypes with higher pri-miR-218-1/2 expression (i.e. MMC), the de-repression magnitude of both semi-log and exponential regulons was greater than levels of de-repression in the PGCb subtype that expresses low levels of pri-miR-218-1/2 (Figure 7J). Furthermore, semi-log and exponential regulons exhibited significantly different dose-dependent relationships with pri-miR-218-1/2 expression, consistent with dose-response curves identified in our allelic series of mice expressing varied levels of miR-218. Therefore, the level of pri-miR-218-1/2 has a dynamic and differential impact upon distinct miR-218 target mRNAs among subtypes of motor neurons. Conversely, the indirect regulon demonstrated increasing de-activation in DKO versus WT motor subtypes with higher pri-miR-218-1/2 expression (Figure 7K and S7L and S7M). Thus, intrinsic variation in the transcription of pri-miR-218-1/2 results in differential regulation of miR-218 dose-sensitive regulons across motor subtypes.

Discussion

Wide ranges in the expression of miRNAs are frequently observed across cell types, development, and disease states and miRNA cellular dose is affected by diverse processes (de Rie et al., 2017; Ha and Kim, 2014; Karreth et al., 2015; Kleaveland et al., 2018; Neilson et al., 2007; Ruegger and Grosshans, 2012). Yet, miRNAs' *in vivo* biological and gene regulatory functions are almost exclusively investigated in all-or-nothing experimental paradigms due to inherent challenges in altering miRNA levels in animals. Prior *in vitro* investigations have suggested miRNA dose can affect the repression of targets in unanticipated ways (Narayan et al., 2017; Shu et al., 2012), and an investigation into the miR-17~92 cluster in B cells observed non-overlapping sets of mRNA targets detected when the miRNAs within this cluster were knocked out versus over-expressed (Jin et al., 2017). These findings have provided clues that modulation of miRNA dose might have non-linear effects on target repression. However, the phenotypic and gene regulatory consequences of miRNA dose on endogenous targets *in vivo* have been largely unexplored (Cassidy et al., 2013). Here, we comprehensively and systematically examine the impact of miR-218 dose upon motor neuron gene expression and phenotypes using combinatorial mouse genetics. This particular miRNA and *in vivo* cellular context are relevant to our understanding of miRNA-mediated disease pathogenesis, as miR-218 is required for neuromuscular synaptogenesis and murine survival and is reduced in ALS patient post-mortem tissues. By transcriptionally profiling motor neurons expressing five distinct levels of miR-218, we found that motor function is closely aligned with a hidden dose-dependent inflection point in the regulation of a subset of exponentially dose-responsive miR-218 targets.

While parsing the varied functions of master gene regulators such as miRNAs is a formidable challenge, our work points to the utility of modulating miRNA dose to disentangle phenotypic effects from multiple, dynamically affected gene networks. We unexpectedly uncovered wide variance in the dose-responsiveness of individual miR-218 target mRNAs and we identify and contrast three uniquely affected gene sets: semi-log, exponential and indirect regulons. The semi-log regulon exhibits uniform and incremental repression proportional to the increase in miR-218 expression level. By contrast, the exponential regulon was greatly repressed by low levels of miR-218, but quickly shifted to a dose-unresponsive state at a dose threshold where repression was saturated. A fundamental implication of these findings is that variations in the dose level of a single miRNA can exert dynamic regulatory effects. For example, a miRNA may repress many targets with equal magnitude at one dose, though the relative repression levels of the same targets could be widely different at another miRNA dose, resulting in non-ratiometric gene regulatory effects within members of a target gene network. Relatedly, we find that semi-log and exponential regulons are similarly repressed in MMC (miR-218 high) motor neurons whereas their relative repression levels are different in PGCb (miR-218 low) motor neurons. Thus, miRNA dose contributes to transcriptional diversity of neuronal populations.

Additionally, we found that miR-218 activates an indirect regulon of peripheral neuron-associated genes with similar magnitude to the most strongly affected direct miR-218 targets. We and others hypothesize that miRNA-mediated indirect effects could be the result of direct repression of a repressor or more complex gene network effects (McGeary et al., 2019). We examined if any miR-218 target genes are themselves repressors that could explain the downstream activation of the indirect regulon. However, no clear candidates could be identified (data not shown). The pathways of indirect miRNA-mediated gene activation are not well understood and warrant further investigation. While biological phenotypes are typically attributed to the direct repressive effects of a miRNA on target mRNAs, miRNAs might modulate coherent downstream gene networks with cellular functions potentially as impactful as those mediated by the directly repressed targets.

Motor neurons and peripheral DRG neurons are two embryonically and functionally distinct neuronal types. Unexpectedly, we found that motor neurons and DRG neurons are co-enriched for indirect regulon genes, which was surprising because these genes depend on miR-218 in motor neurons while DRG neurons lack miR-218. Analogous to convergent evolution, motor neurons use miR-218 while DRGs must use alternative gene regulatory pathways to activate the same gene set. Thus, it is possible miR-218 arose as a mechanism to activate genes that contribute to peripheral axonal and synaptic functions in CNS-derived motor neurons.

Computational target prediction approaches have enabled a deeper understanding of miRNA-mediated gene networks and biological functions, though the most advanced models capture only a fraction of experimentally observed repressive effects (Agarwal et al., 2015; McGeary et al., 2019). While noise and opposing indirect effects have been proposed to explain model inaccuracies, our data demonstrates that miRNA repressive effects upon particular mRNA targets may only be observed at certain dose ranges. Examination of miRNA targets at low or high expression levels (i.e. as occurring with miRNA knockdown

versus over-expression) might bias the detection of miRNA-mediated effects for targets with either semi-log or exponential responses (Figure S7N and S7O). Incorporation of target mRNA dose response parameters could greatly improve the accuracy of prediction models and their application to biological systems. Additionally, we find high correlations of dose responsiveness with 3'UTR-mediated characteristics including the number of miR-218 binding sites, length, abundance, and sub-cellular localization, suggesting miRNA dose-responses may be closely tied to RNA metabolic pathways rather than simply stoichiometry or strength of base pair matching of seed sequences. Our results suggest dose response variations are due to intrinsic 3'UTR differences of individual mRNA transcripts, though complex feedforward gene regulatory effects could also contribute to these distinctions. By using genome editing to manipulate MRE number, 3'UTR length, and subcellular localization signals independent of other variables, the impact of these features on miRNA dose responsiveness might be elucidated. Further work is needed to understand potentially wide-ranging influences contributing to distinct miRNA dose-responses of individual target mRNAs.

The combinatorial and sequential action of developmentally expressed gene regulators are often conceptualized as driving cell fate decisions between discrete states (Waddington, 1957). In contrast, we find that miR-218 can dose-sensitively adjust motor neuron gene signatures along a continuum. Rather than reaching a distinct equilibrium, miR-218-mediated regulation of motor neuron gene networks is highly dynamic – and surprisingly unstable. This is most clearly evident from our observation that dose-responses can have steep inflection points and that regulons have widely ranging repression levels among motor neuron subtypes. Based upon these findings, we hypothesize that subsets of miRNA targets may be particularly sensitive to hidden miRNA dose thresholds that may be associated with disease states. Indeed, miRNA dysregulation is frequently associated with nervous system disorders, well-illustrated by nonsyndromic, progressive hearing loss caused by haploinsufficiency of miR-96, a miRNA highly enriched in mechanosensory hair cells of the inner ear (Mencia et al., 2009; Solda et al., 2012; Weston et al., 2006). Patients' symptom severity ranged from mild in adolescence to profound with advanced age, suggesting partial reduction in miR-96 expression and aging synergistically cause deterioration of sensory function.

Likewise, we propose that reductions in miR-218 expression may contribute to neurodegeneration of motor neurons in ALS patients in the setting of aging and inherited mutations causing dysfunction in miRNA metabolism. ALS typically has a much greater impact on somatic motor neurons than visceral (PGC) subtypes. An interesting feature that emerges from our single cell analysis is that somatic and visceral motor neuron transcriptomes are distinct at baseline and have different magnitudes of effect by miR-218. Specifically, somatic motor neurons are more strongly affected by miR-218 than visceral motor neurons, potentially contributing to motor neuron subtype-specific effects in ALS. Consistent with the plausibility that miR-218 dysregulation contributes to ALS, motor neuron diseases are frequently associated with genomic mutations in RNA binding proteins such as FUS, TDP43, and SMN involved in miRNA biogenesis (Nussbacher et al., 2019; Volonte et al., 2015). These genes are ubiquitously expressed, raising questions of why motor neurons are particularly vulnerable to perturbations in RNA processing pathways

under their control. miR-218's highly motor neuron-selective expression, dose-sensitive effects on gene regulation and neuromotor function, greater effects in somatic versus visceral subtypes, and downregulation in ALS spinal tissue raise intriguing possibilities for a potential role in motor neuron disorders.

STAR Methods

RESOURCE AVAILABILITY

Lead Contact—Further information and requests for resources and reagents should be directed to and will be fulfilled by the Lead Contact, Sam Pfaff (pfaff@salk.edu).

Materials Availability—Mouse lines generated in this study are available upon request.

Data and Code Availability—The bulk and single cell RNA sequencing data sets generated during this study are publicly available at ArrayExpress accession: E-MTAB-10571. Processed data is available in supplemental tables. Any additional information required to reanalyze the data reported in this paper is available from the lead contact upon request.

EXPERIMENTAL MODEL AND SUBJECT DETAILS

Mice—Microinjection of linearized plasmids into pronuclei for generating transgenic mice (tg(ILOp(908bp)::eGFP-218-2)) was performed at the Salk Transgenic Core Facility. To generate the 218-2$^{\Delta ILO}$ mouse allele, mouse oocytes were microinjected with Cas9 mRNA:gRNA:gRNA mixtures (at concentrations of 30ng/uL:15ng/uL:15ng/uL) and were re-implanted into B6D2F1 pseudo-pregnant females. Successful multiplexed deletions were detected by PCR genotyping of mouse tails and confirmed by Sanger sequencing (Eton Biosciences). Mouse lines were maintained in a CB6F1/J background. The allelic series of mice were generated by crossing mice carrying the Hb9::gfp reporter (Pfaff Lab) with previously generated mouse alleles (218-1 KO and 218-2 KO) (Amin et al., 2015) and the newly generated 218-2$^{\Delta ILO}$ allele. For FACS isolation of embryonic motor neurons, only one parent carried the *Hb9::gfp*+ allele (assessed by genotyping by Transnetyx, Inc.) so that each Hb9::gfp+ embryo would only carry one copy of the fluorescent allele. FACS-isolated motor neurons for each RNA sequencing sample (bulk and single cell) were isolated from only one embryo and none were pooled. Both male and female mice were used in all studies. When used, littermates are documented in the text and figures. Genotyping authentication was performed using services from Transnetyx, Inc. Mice were maintained on a 12:12 hour light:dark cycle and provided *ad libitum* access to food and water. All mouse work was conducted in accordance with IACUC guidelines of the Salk Institute for Biological Studies.

Cell lines—*Hb9::gfp* mES line (Lee et al., 2004) was cultured on MEF feeders using standard embryonic stem cell culture techniques. In brief, mES cells were passaged as needed using 0.25% trypsin (Life Technologies) and passaged in FCS media ([Knockout DMEM (Thermofischer Scientific), 1X HEPES (Life Technologies), 1X non-essential amino acids (Life Technologies), 200 mM L-glutamine (Life Technologies), 10% ES-qualified fetal bovine serum (Millipore), 0.1 mM β-mercaptoethanol (Sigma), 1,000–2,000

units of leukemia inhibitory factor (LIF) (Calbiochem), 1X Antibiotic-Antimycotic (Life Technologies)]). When feeding and not passaging, cells were fed with FCS media with Knockout Serum Replacement (Thermofischer Scientific) replacing FCS. To generate spinal cord neurospheres, mESCs were dissociated with trypsin and 10^6 cells were plated in suspension in 10cm low-attachment dishes in ADFNK media [ADFNK media [Advanced D-MEM/F-12 (Life Technologies): Neurobasal medium (Life Technologies) (1:1), 10% Knockout Serum Replacement (Life Technologies), 200 mM L-Glutamine (Life Technologies), and 0.1 mM b-mercaptoethanol (Sigma)]. After two days, generated embryoid bodies were split onto three new 10-cm plates with fresh ADFNK media supplemented with 1 μM all-trans retinoic acid (RA, Sigma) and 100 nM smoothened agonist (SAG, Calbiochem). Two days later, freshly supplemented media was exchanged (Sternfeld et al., 2017).

Human spinal samples—Frozen control human spinal samples were dissected post-mortem, embedded in OCT and stored at 80°C until tissue processing, courtesy of John Ravits (UCSD). Controls had documented causes of death unrelated to spinal neuropathology and were of ages 49 to 77 years old. Frozen blocks were cryosectioned on a Leica CM1850 cryostat. miRNA in situ hybridizations were performed on tissue sections using a 5'/3'-DIG prelabelled miR-218 or miR-124 LNA probes. Briefly, tissues were fixed with 4% PFA for 10 minutes, washed in PBS, and treated with proteinase K (New England Biolabs) for 10 minutes. Sections were fixed again in 4% PFA, washed in PBS and acetylated in acetic acid. Sections were incubated with 50nM DIG labelled probes in hybridization buffer overnight before sequential washes in 5x, 1x, and 0.2x SSC, incubation with anti-DIG antibodies conjugated with alkaline phosphatase (Roche), washes in PBS, and development of the color reaction in NBT/BCIP (Roche).

METHODS DETAILS

Systematic review of miRNA profiling studies in ALS patients—Pubmed was searched for combinations of the following search terms: microRNA, miRNA, miR, ALS, amyotrophic lateral sclerosis, spinal cord, motor neuron, human, neural tissue, profiling, sequencing, microarray, taqman, nanostring, laser capture. Last search was performed in March of 2020. We report all published manuscripts that involved the profiling of miRNAs of spinal neural tissue from ALS patients and controls - none were excluded. Statistics and differential expression values are presented as reported in the original manuscript.

Generation and isolation of CRISPR-modified mES-MNs—*Hb9::gfp* mES line (Lee et al., 2004) was cultured on MEF feeders using standard embryonic stem cell culture techniques. mESCs were transfected with Lipofectamine 2000 with two pX330 vectors (containing Cas9 and two individual guide RNAs) and a plasmid expressing a puromycin resistance cassette. Guide RNAs were chosen to create specific multiplexed deletions between the selected gRNAs. 18 hours after transfection, mESCs were treated with puromycin for 48 hours to select for transfected cells. mESCs were split onto 10cm dishes with low density to allow for single colony selection. Colonies were manually picked after 5-8 days, manually dissociated, and split onto a feeder free gelatin coated plate for genotyping and MEF feeders for continued culture and freezing. Colonies were screened

by PCR for wild type and knockout mutations to identify homozygous deletions of the indicated genomic regions. Selected mES lines that passed two rounds of PCR screening were expanded. On day 6 of spinal neurosphere differentiation, neurospheres containing *Hb9::gfp*+ motor neurons were dissociated with papain (Worthington Biochemical), passed through a 40μm filter, and the resulting single cell suspension was used for fluorescence activated cell sorting. Cells were sorted on a Becton Dickinson FACS Vantage SE DiVa using Coherent Sapphire 488nm solid state lasers (200mW) and collected directly into Trizol LS. RNA was isolated according to Trizol LS protocol.

***In situ* hybridization and immunohistochemistry—**Microdissections of mouse tissues were performed under a Zeiss Stemi SV6 microscope, and imaging was performed with a Leica confocal CTR6500 (TCS SPE) microscope or Zeiss Lumar V12 stereomicroscope. Briefly, tissue was fixed in 4% PFA for 2 hours at 4°C, washed in PBS, cryoprotected in 30% sucrose for 1 hour before mounting and freezing in O.C.T. compound (Tissue-Tek). Frozen blocks were cryosectioned on a Leica CM1850 cryostat onto Superfrost microscope slides (Thermo Scientific). Antibodies: Rabbit anti-Neurofilament M (Chemicon AB1987), alpha-bungarotoxin- 3 tetramethylrhodamine for AChR labelling (Life Technologies T-1175), rabbit anti-Synaptophysin (Santa Cruz: sc-9116). Images were acquired using an Olympus FV3000. Images are presented as z-projections. Images of P4 spinal cord *in situ* hybridization were obtained from the Allen Spinal Cord Atlas (Henry and Hohmann, 2012).

RNAscope—Vertebral columns and adjacent tissue (including DRG) of E18 WT and DKO embryos were collected, genotyped, and fresh frozen in 2:1 OCT:20% sucrose on dry ice. To limit technical variance, tissues of both genotypes were cryosectioned (16μm) onto the same glass slide prior to performing RNAscope Fluorescent Multiplex Assay v1. Manufacturer's instructions were followed except for 1:10 dilution of protease IV in PBS was applied for a 20 minute incubation. Localization of ChAT and Prph were performed in parallel.

In Ovo Electroporation—Chick eggs (Charles River and McIntyre Farms) were incubated in a humidified chamber, and embryos were staged according to HH. DNA constructs were injected into the lumens of HH stage 18–19 chick embryonic spinal cords. Electroporation was performed using a square wave electroporator (BTX). Chick embryos were harvested and analyzed after 48 hr.

CRISPR/Cas9-mediated deletion in mice—Pre-miR-218-2 ILO knockout mice were generated using CRISPR/Cas9 targeting, as described (Wang et al., 2013). Briefly, Cas9 mRNA was *in vitro* transcribed, capped and polyadenylated (mMachine kit, Invitrogen). Guide RNAs were designed using CRISPR Design (MIT) to decrease the likelihood of off-target effects and were in vitro transcribed using the New England Biolabs High Yield In Vitro Transcription Kit (guide sequences available in Table S1). Mouse oocytes were microinjected with Cas9 mRNA:gRNA:gRNA mixtures (at concentrations of 30ng/uL:15ng/uL:15ng/uL) and were re-implanted into B6D2F1 pseudo-pregnant females.

Embryonic motor neuron isolation—Spinal cords were micro-dissected (Leica stereomicroscope) from E12.5 mice carrying a single *Hb9::gfp*+ allele and were dissociated

with papain (papain dissociation kit, Worthington Biochemical) for 30 minutes. Tail clips were simultaneously taken from each embryo for genotyping. Spinal tissue was triturated and centrifuged at 1000rpm for 5 minutes. Dissociated cells were resuspended in 1:1 Neurobasal:DMEM/F12 (without phenol red) with 3% Horse Serum (Invitrogen) and DNase (Worthingon Biochemical) and were passed through a 35μm cell strainer (08-771-23, BD Falcon). Cells were sorted on a Becton Dickinson FACS Vantage SE DiVa using Coherent Sapphire 488nm solid state lasers (200mW) and collected directly into Trizol LS. Sorted samples were stored at −80C. Total RNA was isolated using the Trizol-LS protocol. miR-218 levels were assessed by Taqman qPCR normalized to the average Ct of two controls: U6 and miR-124.

Bulk RNA sequencing—RNA sequencing and gene expression quantification mRNA sequencing libraries were prepared using the *TruSeq RNA Library Preparation Kit (v2)* according to the manufacturer's instructions (Illumina). Briefly, RNA with polyA+ tails was selected using oligo-dT beads. mRNA was then fragmented and reverse-transcribed into cDNA. cDNA was end-repaired, index adapter-ligated and PCR amplified. AMPure XP beads (Beckman Coulter) were used to purify nucleic acids after each step. Small RNA-sequencing libraries were prepared using NEBNext Small RNA Library Prep for Illumina. Briefly, 3' adapter was ligated to total RNA, any excess 3' adaptor was quenched by hybridization of reverse transcription primer to prevent primer dimers. RNA was then ligated to 5' adaptor, reverse transcribed and PCR amplified. Libraries were then quantified, pooled and sequenced using either the Illumina HiSeq 2500 or Illumina HiSeq 2000 platforms at the Salk NGS Core.

Single cell RNA-seq—The entire E12 spinal cord was dissected from a single *Hb9::gfp*+ embryo per sample. To identify DKO embryos (from Hb9::gfp+;miR218-1−/−;miR218-2−/+ x miR218-1−/−;miR218-2−/+ crosses), embryo tails were genotyped concurrently during the spinal dissociation process. WT embryos were collected from crosses of WT mice. Duplicates were obtained from two embryos within the same litter. Cell dissociation was conducted using Papain following the manufacturer's instruction (Worthington Biochemical) (Osseward et al., 2021). Specifically, spinal cords were placed in 1mL papain solution in 37C water bath for 20 minutes, gently triturated, incubated again for additional 25 minutes, fully triturated, and quenched with 250 uL ovomucoid solution. Dissociated cells were then spun down at 150 rcf for 5 minutes. The cell pellet was resuspended in 5% FCS in DMEM/F12 with HEPES without phenol red, and the cells were passed through a 40 micron cell strainer. Via FACS (FACSDIVA, BD), 20,000 cells were collected (gated for GFP) into 500 uL of 5% FCS with DMEM/F12 with HEPES without phenol red. Sorted cells were spun down at 300 rcf for 2 minutes, and 370uL were removed to leave remaining 130 uL. The cells were resuspended in this remaining media. 32.5uL of the resuspended cells (~3,000 cells) were loaded into 10X Chromium Controller using Chromium Single Cell 3' v2 reagents. Sequencing libraries were prepared following the manufacturer's instructions (10X Genomics). 14 cycles were used for cDNA amplification, and 10 cycles were used for library amplification. The resulting sequencing library was sequenced with Paired End reads, with a Read 1 of 26 basepairs and a Read 2 of 98 basepairs, on an Illumina HiSeq 4000 at the UCSD IGM Genomics Center.

QUANTIFICATION AND STATISTICAL ANALYSIS

Bulk RNA sequencing analysis—Raw sequencing data was de-multiplexed and converted into FASTQ files using CASAVA (v1.8.2). FASTQ files were inspected with FastQC (Galaxy Version 0.72). Read visualization was performed with HISAT2 (Galaxy Version 2.1.0+galaxy3) and bamCoverage (Galaxy Version 3.1.2.0.0) conversion into bigwig file, visualized within UCSC genome browser or IGV (Broad Institute). TPM were generated with Kallisto (Galaxy Version 0.43.1.3) using GENCODE VM18 as reference transcriptome. Normalized counts were obtained using DESeq2 (Galaxy Version 2.11.40.2), mapping transcripts to gene symbols (41378 unique gene symbols) across all 15 samples (WT, 1KO, 2KO, 1KO;$2^{-/\Delta ILO}$, DKO, n=3,3,3,3,3). Only protein coding genes with nonzero normalized counts across were included for PCA plotting of miR-218 knockout backgrounds (15 samples, 14059 genes) and DRG versus interneuron populations versus WT motor neurons vs DKO motor neurons (13 samples, 14092 genes). Data was log-transformed prior to clustering with ClustVis (row scaling by unit variance, PCA method: SVD with imputation). ChIP sequencing (Lhx3, Isl1, Onecut1 and H3K27ac) and ATACseq data from motor neurons were mapped with BWA (Galaxy Version 0.7.17.4), replicates were merged, and reads were visualized with UCSC genome browser (Rhee et al., 2016).

Sylamer—FASTA of 5'UTR, CDS, and 3'UTR sequences obtained from UCSC Table Browser for GENCODE_VM18 database with masked repeats with "N". 51370 3'UTR sequences were obtained with corresponding gene symbol. For genes with multiple isoforms, the longest UTR sequence among annotated transcripts per gene was retained. The top 10,000 highest expressed genes were included in analysis. These genes were ranked from most enriched in wild type to miR-218-DKO motor neurons, as determined by DESeq2. Sequence files and ranked gene lists were used with Sylamer software (Enright Lab) - 8mer search (markov correction: 5), 7mer search (markov correction: 4), and 6mer search (markov correction: 4) including known miRNA seed sequences.

miR-218 target identification—miR-218 predicted targets were obtained from TargetScan Release 7.2 (August 2018 version). Of 4750 transcripts with predicted binding sites (irrespective of site conservation), 4711 transcripts were matched to transcript identifiers either in GENCODE VM18 or by gene symbol. Targets with a cumulative weighted context++ score <(−0.15) were retained (cutoff empirically determined, lower negative scores indicative of stronger prediction of miR-218 targeting). Only genes with base mean expression >10 from DESeq2 (DKO v WT, n=3,3) were retained for identification of miR-218 target genes. P-values obtained from DESeq2. Differential expression of 959 genes were examined based upon criteria above, 316 passed significance $p<0.05$ and were de-repressed in the DKO samples. Hierarchical clustering by on correlation was performed on miR-218 targets' gene expression (biological triplicates averaged) using Morpheus (Broad Institute).

Dose-response regression—All regressions were performed on each miR-218 target gene's expression (DESeq2 normalized counts, average of biological replicates) against miR-218 expression (as assessed by Taqman qPCR versus U6 and miR-124 as controls) in each genotype using GraphPad Prism 7.03. Semi-log regression and one-phase association

curves were used for the semi-log and exponential regulons, respectively. Representative genes are shown with regression curves and 95% CI. Semi-log regulon genes are defined as miR-218 targets that fit a semi-log regression with adj r^2>0.95. Exponential regulon genes are defined as miR-218 targets that 1) are not part of the semi-log regulon, 2) fit a one-phase association regression with adj r^2>0.95, and 3) fit a one-phase association significantly better than a semi-log regression (extra sum of squares test). Comparisons of fold change, context++ score, UTR length, #MREs and base mean expression were performed on n=41,49 genes in the semi-log and exponential regulons with adj. p-value >0.95. Comparisons of soma/axonal enrichment were performed by cross-referencing regulon genes with soma/axonal enrichment values from (Nijssen et al., 2018). Go term enrichment was performed with Metascape (Default parameters, only Biological Processes Go Terms). Half-max repression by miR-218 was determined from DESeq2 normalized counts averaged across biological triplicates, and the level of miR-218 expression at which gene expression was repressed by 50% of maximal observed repression from WT to DKO geneotypes. Half-max repression values could not be calculated accurately for five of the 316 target genes due to noise around the 50% repression point and were excluded.

Single cell RNA sequencing analysis—Raw sequencing data was demultiplexed using bcl2fastq v2.18.0.12. Sequencing and demultiplexing of biological samples into FASTQ format files were performed by the UCSD sequencing core. Reads from the four samples were aligned and quantified separately for gene expression using Cellranger version 3 (10x Genomics) using the mm10 mouse transcriptome annotation. Samples were combined into a single expression matrix using Cellranger's 'aggr' program by equalizing aligned read counts and we used the estimated cell count from Cellranger for downstream analysis. The resulting UMI matrix (9,043 cells) and sample identities were imported into R. To filter out low quality cells and doublets we generated a histogram of the number of detected features per-cell and selected lower and upper bounds that retained the dominant population of cells. We also observed a histogram of the percentage of mitochondrial gene expression per cell and selected an upper limit of 8%. These two filters removed 796 cells leaving 8,247 cells for downstream analysis.

Dimensionality Reduction—Highly variable genes (HVG) were identified using a method previously described (Brennecke et al., 2013) with FDR=0.1. PCA was performed on normalized and log2+1 scaled UMI using the identified HVGs. Normalization was performed by dividing each cell's UMI counts by its respective total UMI count across all genes and scaling by 10,000, resulting in an expression value comparable to TPM in bulk RNAseq. Significant components were identified automatically by comparing the eigenvalues to the 95th percentile of the appropriate Wishart distribution. Significant principal components were provided as input for the UMAP transform (umap package, R). We used 'n_neighbors=20' for UMAP generation and default settings. Dimensionality reduction was performed separately for both all cells and the interneuron-excluded subset.

Neuron subtype identification—Interneuron, motor neuron, neuron subtype, rostro-caudal, and column identities were detected by comparing with the expression of known marker genes for each subtype in each cell. This was done by first, assembling markers for

each neuron subtype based on known expression of transcription factor and neurotransmitter markers (Alaynick et al., 2011). The UMI count matrix was binarized using a threshold of >= 1 UMI as “detected” and reduced to the marker genes. A second matrix was constructed (marker genes by subtype identity) and Euclidean distances between cells and the subtype identity matrix were calculated. For each cell the best match (lowest Euclidean distance) was selected as the cell’s identified subtype. We identified 6,328 motor neurons and 1,919 interneurons. Rostral/caudal identity was detected using Hox gene expression from known Hox code expression patterns and published spinal cord region bulk RNAseq from multiple rostro-caudal regions (Hayashi et al., 2018). TPM scaled expression of Hox genes was cross-correlated with the normalized UMI counts for corresponding Hox gene expression in the single-cell data. For each cell, the rostro-caudal region with the highest correlation value was identified. In the case of no correlation (i.e. none of the genes expressed in a single cell) or when a cell correlated equally well to more than one type, we excluded the cell from downstream analysis involving rostral/caudal identity. Column type identity was detected using known positive and negative markers (Alaynick et al., 2011) within a motor neuron specific subpopulation, the predicted rostral/caudal identity, and the UMAP clustering of the cells. Initial type calls were made using markers alone and were refined based on the UMAP layout and their identified rostral/caudal identities. We were unable to call column types for 216 cells which were marked as ambiguous and excluded from subtype analyses.

Pseudo-bulk comparisons—To compare and perform differential gene expression between identified neuronal populations based on the source sample, known genotype, and predicted neuronal identity, we summed the expression of individual cells on the gene level into pseudo-bulk expression tables. The pseudo-bulk expression data were treated like bulk RNA-seq for normalization and differential expression testing performed using DESeq. Reads that mapped to the Slit2/3 gene body were annotated as pri-miR-218-1/2 as we previously found that most RNA sequencing reads from motor neurons map to the latter (Amin et al., 2015). We aligned bulk RNAseq WT motor neuron reads to the mouse genome (mm10) using STAR and assembled de-novo motor neuron transcripts using Stringtie which correctly assembled motor neuron pri-miR-218-1/2 isoforms that were not present in currently available transcriptome annotations. We used the assembly with motor neuron-specific pri-miR-218-1/2 isoforms to build an alignment index for Kallisto and quantified each of the four scRNA seq samples with the Kallisto/BUS pipeline.

Pseudo-time analysis—Pseudo-time analysis was performed using functions provided by the Monocle2 package for R. We identified the top 1000 variable genes using Seurat’s highly variable feature calling method and ran Monocle’s pseudo-time pipeline following using default option.

Statistical representation in figures—Error bars represent SEM except as otherwise stated. Boxplots range from 10-90%iles with outliers represented as individual points. Statistical details may be found as otherwise stated in figure legends. P-values are listed in figure panels when significant. No datasets obtained were excluded prior to or during analysis.

Supplementary Material

Refer to Web version on PubMed Central for supplementary material.

ACKNOWLEDGMENTS

We thank: Karen Lettieri and Miriam Gullo (Salk Institute) for mouse husbandry; Marito Hayashi (Harvard Medical School) for helpful discussions; Yelena Dayn (Salk Institute; NIH-NCI CCSG: P30 014195) for mouse oocyte injections; Flow Cytometry Core Facility (Salk Institute; NIH-NCI CCSG: P30 014195 and Shared Instrumentation Grant S10-OD023689 (Aria Fusion cell sorter); The Salk Institute Next Generation Sequencing Core (Nasun Hah and other members; NIH-NCI CCSG: P30 014195, the Chapman Foundation and the Helmsley Charitable Trust), the UCSD IGM Genomic Center (Kristen Jepsen and other members); John Ravits (UCSD) for ALS tissue sample bank. S.L.P. is a Benjamin H. Lewis chair in neuroscience. N.D.A. is supported by the NIMH T32 Training Grant T32MH019938 and the Stanford Department of Psychiatry and Behavioral Sciences. D.B. is supported by the Giovanni Armenise-Harvard Foundation Career Development Award. Additional funding sources: National Institutes of Health (1 R03 NS121480-01 and 1 R21 NS121846-01), TargetALS, and The Department of Defense (ALSRP (TIA) W81XWH1810120).

References

Afgan E, Baker D, Batut B, van den Beek M, Bouvier D, Cech M, Chilton J, Clements D, Coraor N, Gruning BA, et al. (2018). The Galaxy platform for accessible, reproducible and collaborative biomedical analyses: 2018 update. Nucleic Acids Res 46, W537–W544. [PubMed: 29790989]

Agarwal V, Bell GW, Nam JW, and Bartel DP (2015). Predicting effective microRNA target sites in mammalian mRNAs. Elife 4.

Alaynick WA, Jessell TM, and Pfaff SL (2011). SnapShot: spinal cord development. Cell 146, 178–178 e171. [PubMed: 21729788]

Amin ND, Bai G, Klug JR, Bonanomi D, Pankratz MT, Gifford WD, Hinckley CA, Sternfeld MJ, Driscoll SP, Dominguez B, et al. (2015). Loss of motoneuron-specific microRNA-218 causes systemic neuromuscular failure. Science 350, 1525–1529. [PubMed: 26680198]

Bartel DP (2018). Metazoan MicroRNAs. Cell 173, 20–51. [PubMed: 29570994]

Brennecke P, Anders S, Kim JK, Kolodziejczyk AA, Zhang X, Proserpio V, Baying B, Benes V, Teichmann SA, Marioni JC, et al. (2013). Accounting for technical noise in single-cell RNA-seq experiments. Nat Methods 10, 1093–1095. [PubMed: 24056876]

Brose K, Bland KS, Wang KH, Arnott D, Henzel W, Goodman CS, Tessier-Lavigne M, and Kidd T (1999). Slit proteins bind Robo receptors and have an evolutionarily conserved role in repulsive axon guidance. Cell 96, 795–806. [PubMed: 10102268]

Buratti E, De Conti L, Stuani C, Romano M, Baralle M, and Baralle F (2010). Nuclear factor TDP-43 can affect selected microRNA levels. FEBS J 277, 2268–2281. [PubMed: 20423455]

Butovsky O, Jedrychowski MP, Cialic R, Krasemann S, Murugaiyan G, Fanek Z, Greco DJ, Wu PM, Doykan CE, Kiner O, et al. (2015). Targeting miR-155 restores abnormal microglia and attenuates disease in SOD1 mice. Ann Neurol 77, 75–99. [PubMed: 25381879]

Butti Z, and Patten SA (2018). RNA Dysregulation in Amyotrophic Lateral Sclerosis. Front Genet 9, 712. [PubMed: 30723494]

Campos-Melo D, Droppelmann CA, He Z, Volkening K, and Strong MJ (2013). Altered microRNA expression profile in Amyotrophic Lateral Sclerosis: a role in the regulation of NFL mRNA levels. Mol Brain 6, 26. [PubMed: 23705811]

Carroll AP, Tooney PA, and Cairns MJ (2013). Context-specific microRNA function in developmental complexity. J Mol Cell Biol 5, 73–84. [PubMed: 23362311]

Cassidy JJ, Jha AR, Posadas DM, Giri R, Venken KJ, Ji J, Jiang H, Bellen HJ, White KP, and Carthew RW (2013). miR-9a minimizes the phenotypic impact of genomic diversity by buffering a transcription factor. Cell 155, 1556–1567. [PubMed: 24360277]

Cheng Y, Wang ZM, Tan W, Wang X, Li Y, Bai B, Li Y, Zhang SF, Yan HL, Chen ZL, et al. (2018). Partial loss of psychiatric risk gene Mir137 in mice causes repetitive behavior and impairs sociability and learning via increased Pde10a. Nat Neurosci 21, 1689–1703. [PubMed: 30397325]

de Rie D, Abugessaisa I, Alam T, Arner E, Arner P, Ashoor H, Astrom G, Babina M, Bertin N, Burroughs AM, et al. (2017). An integrated expression atlas of miRNAs and their promoters in human and mouse. Nat Biotechnol 35, 872–878. [PubMed: 28829439]

Emde A, Eitan C, Liou LL, Libby RT, Rivkin N, Magen I, Reichenstein I, Oppenheim H, Eilam R, Silvestroni A, et al. (2015). Dysregulated miRNA biogenesis downstream of cellular stress and ALS-causing mutations: a new mechanism for ALS. EMBO J 34, 2633–2651. [PubMed: 26330466]

Figueroa-Romero C, Hur J, Lunn JS, Paez-Colasante X, Bender DE, Yung R, Sakowski SA, and Feldman EL (2016). Expression of microRNAs in human post-mortem amyotrophic lateral sclerosis spinal cords provides insight into disease mechanisms. Mol Cell Neurosci 71, 34–45. [PubMed: 26704906]

Geaghan M, and Cairns MJ (2015). MicroRNA and Posttranscriptional Dysregulation in Psychiatry. Biol Psychiatry 78, 231–239. [PubMed: 25636176]

Ha M, and Kim VN (2014). Regulation of microRNA biogenesis. Nat Rev Mol Cell Biol 15, 509–524. [PubMed: 25027649]

Hayashi M, Hinckley CA, Driscoll SP, Moore NJ, Levine AJ, Hilde KL, Sharma K, and Pfaff SL (2018). Graded Arrays of Spinal and Supraspinal V2a Interneuron Subtypes Underlie Forelimb and Hindlimb Motor Control. Neuron 97, 869–884 e865. [PubMed: 29398364]

Henry AM, and Hohmann JG (2012). High-resolution gene expression atlases for adult and developing mouse brain and spinal cord. Mamm Genome 23, 539–549. [PubMed: 22832508]

Inukai S, Pincus Z, de Lencastre A, and Slack FJ (2018). A microRNA feedback loop regulates global microRNA abundance during aging. RNA 24, 159–172. [PubMed: 29114017]

Jin HY, Oda H, Chen P, Yang C, Zhou X, Kang SG, Valentine E, Kefauver JM, Liao L, Zhang Y, et al. (2017). Differential Sensitivity of Target Genes to Translational Repression by miR-17~92. PLoS Genet 13, e1006623. [PubMed: 28241004]

Jung H, Mazzoni EO, Soshnikova N, Hanley O, Venkatesh B, Duboule D, and Dasen JS (2014). Evolving Hox activity profiles govern diversity in locomotor systems. Dev Cell 29, 171–187. [PubMed: 24746670]

Kamal MA, Mushtaq G, and Greig NH (2015). Current Update on Synopsis of miRNA Dysregulation in Neurological Disorders. CNS Neurol Disord Drug Targets 14, 492–501. [PubMed: 25714967]

Karreth FA, Reschke M, Ruocco A, Ng C, Chapuy B, Leopold V, Sjoberg M, Keane TM, Verma A, Ala U, et al. (2015). The BRAF pseudogene functions as a competitive endogenous RNA and induces lymphoma in vivo. Cell 161, 319–332. [PubMed: 25843629]

Kleaveland B, Shi CY, Stefano J, and Bartel DP (2018). A Network of Noncoding Regulatory RNAs Acts in the Mammalian Brain. Cell 174, 350–362 e317. [PubMed: 29887379]

Lee SK, Jurata LW, Funahashi J, Ruiz EC, and Pfaff SL (2004). Analysis of embryonic motoneuron gene regulation: derepression of general activators function in concert with enhancer factors. Development 131, 3295–3306. [PubMed: 15201216]

Magri F, Vanoli F, and Corti S (2018). miRNA in spinal muscular atrophy pathogenesis and therapy. J Cell Mol Med 22, 755–767. [PubMed: 29160009]

Makeyev EV, Zhang J, Carrasco MA, and Maniatis T (2007). The MicroRNA miR-124 promotes neuronal differentiation by triggering brain-specific alternative pre-mRNA splicing. Mol Cell 27, 435–448. [PubMed: 17679093]

Matoulkova E, Michalova E, Vojtesek B, and Hrstka R (2012). The role of the 3' untranslated region in post-transcriptional regulation of protein expression in mammalian cells. RNA Biol 9, 563–576. [PubMed: 22614827]

McGeary SE, Lin KS, Shi CY, Pham TM, Bisaria N, Kelley GM, and Bartel DP (2019). The biochemical basis of microRNA targeting efficacy. Science 366.

Mencia A, Modamio-Hoybjor S, Redshaw N, Morin M, Mayo-Merino F, Olavarrieta L, Aguirre LA, del Castillo I, Steel KP, Dalmay T, et al. (2009). Mutations in the seed region of human miR-96 are responsible for nonsyndromic progressive hearing loss. Nat Genet 41, 609–613. [PubMed: 19363479]

Metsalu T, and Vilo J (2015). ClustVis: a web tool for visualizing clustering of multivariate data using Principal Component Analysis and heatmap. Nucleic Acids Res 43, W566–570. [PubMed: 25969447]

Nam JW, Rissland OS, Koppstein D, Abreu-Goodger C, Jan CH, Agarwal V, Yildirim MA, Rodriguez A, and Bartel DP (2014). Global analyses of the effect of different cellular contexts on microRNA targeting. Mol Cell 53, 1031–1043. [PubMed: 24631284]

Narayan N, Morenos L, Phipson B, Willis SN, Brumatti G, Eggers S, Lalaoui N, Brown LM, Kosasih HJ, Bartolo RC, et al. (2017). Functionally distinct roles for different miR-155 expression levels through contrasting effects on gene expression, in acute myeloid leukaemia. Leukemia 31, 808–820. [PubMed: 27740637]

Neilson JR, Zheng GX, Burge CB, and Sharp PA (2007). Dynamic regulation of miRNA expression in ordered stages of cellular development. Genes Dev 21, 578–589. [PubMed: 17344418]

Nijssen J, Aguila J, Hoogstraaten R, Kee N, and Hedlund E (2018). Axon-Seq Decodes the Motor Axon Transcriptome and Its Modulation in Response to ALS. Stem Cell Reports 11, 1565–1578. [PubMed: 30540963]

Nussbacher JK, Tabet R, Yeo GW, and Lagier-Tourenne C (2019). Disruption of RNA Metabolism in Neurological Diseases and Emerging Therapeutic Interventions. Neuron 102, 294–320. [PubMed: 30998900]

Osseward PJ 2nd, Amin ND, Moore JD, Temple BA, Barriga BK, Bachmann LC, Beltran F Jr., Gullo M, Clark RC, Driscoll SP, et al. (2021). Conserved genetic signatures parcellate cardinal spinal neuron classes into local and projection subsets. Science 372, 385–393. [PubMed: 33888637]

Palanichamy JK, and Rao DS (2014). miRNA dysregulation in cancer: towards a mechanistic understanding. Front Genet 5, 54. [PubMed: 24672539]

Park CY, Choi YS, and McManus MT (2010). Analysis of microRNA knockouts in mice. Hum Mol Genet 19, R169–175. [PubMed: 20805106]

Paul P, Chakraborty A, Sarkar D, Langthasa M, Rahman M, Bari M, Singha RS, Malakar AK, and Chakraborty S (2018). Interplay between miRNAs and human diseases. J Cell Physiol 233, 2007–2018. [PubMed: 28181241]

Philippidou P, and Dasen JS (2013). Hox genes: choreographers in neural development, architects of circuit organization. Neuron 80, 12–34. [PubMed: 24094100]

Rajman M, and Schratt G (2017). MicroRNAs in neural development: from master regulators to fine-tuners. Development 144, 2310–2322. [PubMed: 28676566]

Ramalingam P, Palanichamy JK, Singh A, Das P, Bhagat M, Kassab MA, Sinha S, and Chattopadhyay P (2014). Biogenesis of intronic miRNAs located in clusters by independent transcription and alternative splicing. RNA 20, 76–87. [PubMed: 24226766]

Reichenstein I, Eitan C, Diaz-Garcia S, Haim G, Magen I, Siany A, Hoye ML, Rivkin N, Olender T, Toth B, et al. (2019). Human genetics and neuropathology suggest a link between miR-218 and amyotrophic lateral sclerosis pathophysiology. Sci Transl Med 11.

Rhee HS, Closser M, Guo Y, Bashkirova EV, Tan GC, Gifford DK, and Wichterle H (2016). Expression of Terminal Effector Genes in Mammalian Neurons Is Maintained by a Dynamic Relay of Transient Enhancers. Neuron 92, 1252–1265. [PubMed: 27939581]

Ruegger S, and Grosshans H (2012). MicroRNA turnover: when, how, and why. Trends Biochem Sci 37, 436–446. [PubMed: 22921610]

Sadlon A, Takousis P, Alexopoulos P, Evangelou E, Prokopenko I, and Perneczky R (2019). miRNAs Identify Shared Pathways in Alzheimer's and Parkinson's Diseases. Trends Mol Med.

Shirasaki R, and Pfaff SL (2002). Transcriptional codes and the control of neuronal identity. Annu Rev Neurosci 25, 251–281. [PubMed: 12052910]

Shkumatava A, Stark A, Sive H, and Bartel DP (2009). Coherent but overlapping expression of microRNAs and their targets during vertebrate development. Genes Dev 23, 466–481. [PubMed: 19240133]

Shu J, Xia Z, Li L, Liang ET, Slipek N, Shen D, Foo J, Subramanian S, and Steer CJ (2012). Dose-dependent differential mRNA target selection and regulation by let-7a-7f and miR-17-92 cluster microRNAs. RNA Biol 9, 1275–1287. [PubMed: 22995834]

Shu P, Wu C, Liu W, Ruan X, Liu C, Hou L, Zeng Y, Fu H, Wang M, Chen P, et al. (2019). The spatiotemporal expression pattern of microRNAs in the developing mouse nervous system. J Biol Chem 294, 3444–3453. [PubMed: 30578296]

Solda G, Robusto M, Primignani P, Castorina P, Benzoni E, Cesarani A, Ambrosetti U, Asselta R, and Duga S (2012). A novel mutation within the MIR96 gene causes non-syndromic inherited hearing loss in an Italian family by altering pre-miRNA processing. Hum Mol Genet 21, 577–585. [PubMed: 22038834]

Sternfeld MJ, Hinckley CA, Moore NJ, Pankratz MT, Hilde KL, Driscoll SP, Hayashi M, Amin ND, Bonanomi D, Gifford WD, et al. (2017). Speed and segmentation control mechanisms characterized in rhythmically-active circuits created from spinal neurons produced from genetically-tagged embryonic stem cells. Elife 6.

Suter T, and Jaworski A (2019). Cell migration and axon guidance at the border between central and peripheral nervous system. Science 365.

Thiebes KP, Nam H, Cambronne XA, Shen R, Glasgow SM, Cho HH, Kwon JS, Goodman RH, Lee JW, Lee S, et al. (2015). miR-218 is essential to establish motor neuron fate as a downstream effector of Isl1-Lhx3. Nat Commun 6, 7718. [PubMed: 26212498]

van Dongen S, Abreu-Goodger C, and Enright AJ (2008). Detecting microRNA binding and siRNA off-target effects from expression data. Nat Methods 5, 1023–1025. [PubMed: 18978784]

Volonte C, Apolloni S, and Parisi C (2015). MicroRNAs: newcomers into the ALS picture. CNS Neurol Disord Drug Targets 14, 194–207. [PubMed: 25613506]

Wang H, Yang H, Shivalila CS, Dawlaty MM, Cheng AW, Zhang F, and Jaenisch R (2013). One-step generation of mice carrying mutations in multiple genes by CRISPR/Cas-mediated genome engineering. Cell 153, 910–918. [PubMed: 23643243]

Weston MD, Pierce ML, Rocha-Sanchez S, Beisel KW, and Soukup GA (2006). MicroRNA gene expression in the mouse inner ear. Brain Res 1111, 95–104. [PubMed: 16904081]

Yoo AS, Sun AX, Li L, Shcheglovitov A, Portmann T, Li Y, Lee-Messer C, Dolmetsch RE, Tsien RW, and Crabtree GR (2011). MicroRNA-mediated conversion of human fibroblasts to neurons. Nature 476, 228–231. [PubMed: 21753754]

Zhou Y, Zhou B, Pache L, Chang M, Khodabakhshi AH, Tanaseichuk O, Benner C, and Chanda SK (2019). Metascape provides a biologist-oriented resource for the analysis of systems-level datasets. Nat Commun 10, 1523. [PubMed: 30944313]

Highlights

- miRNA cellular dose is a major determinant of *in vivo* neuronal mRNA target selection
- Modulation of miR-218 levels reveals distinct dose-response curves of target mRNAs
- Motor failure occurs at the miR-218 dose inflection point for an exponential regulon
- Motor neuron subtypes are distinguished by magnitude of miR-218-mediated effects

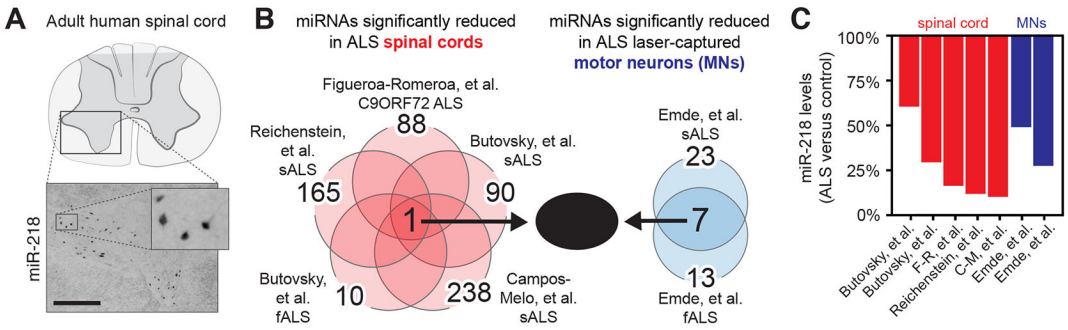

Figure 1.

miR-218 is reduced in ALS patient spinal tissue. (A) miR-218 *in situ* hybridization signal in ventrolateral motor neurons of post-mortem adult human spinal cords. Scale bar, 1mm. (B) Venn diagram of miRNAs significantly reduced in profiling studies of human post-mortem neural tissue (either dissected spinal tissue (red) or laser captured motor neurons (blue) from sporadic (sALS), familial (fALS) and C9ORF72 ALS patients versus controls (Butovsky et al., 2015; Campos-Melo et al., 2013; Emde et al., 2015; Figueroa-Romero et al., 2016; Reichenstein et al., 2019). Only miR-218 was significantly reduced in patients versus controls across all studies, quantified in (C) where miR-218 reduction was between 30% and 90%.

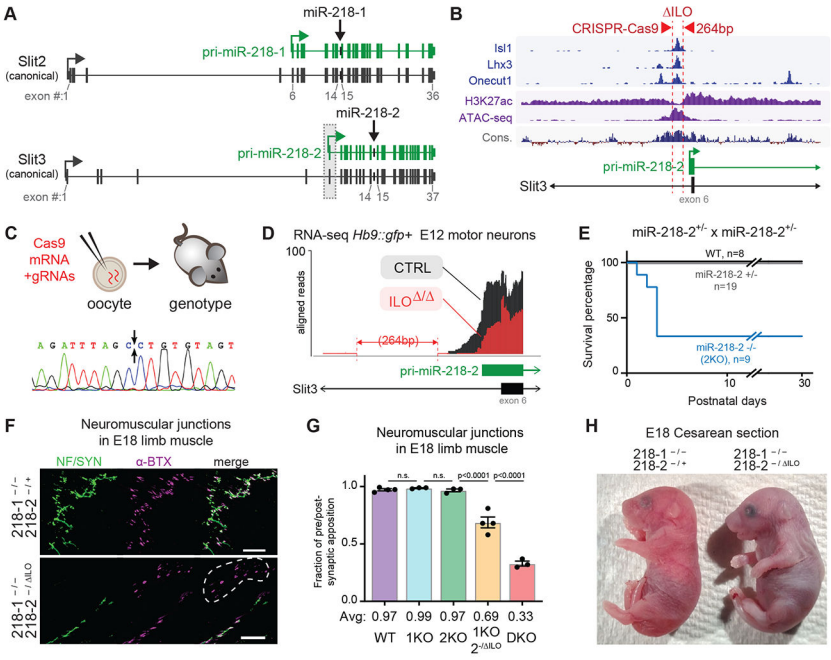

Figure 2.

A miR-218 dose threshold for neuromotor control. (A) miR-218 is expressed via alternative motor neuron-specific promoters (green) encoded within the Slit2 and Slit3 genes. (B) Motor neuron-specifying transcription factor binding sites targeted by CRISPR/Cas9 (Rhee et al., 2016). (C) Mouse oocytes were injected with Cas9 mRNA and gRNAs to generate a 264bp deletion (ΔILO). (D) Overlayed RNAseq reads of control (black) and 218-2$^{\Delta ILO/\Delta ILO}$ (red) motor neurons. (E) miR-218-2 knockout (2KO) mice have a partially penetrant phenotype of early post-natal death. (F) Neurofilament M (NF) and synaptophysin (SYN) staining of pre-synaptic motor axons and alpha-bungarotoxin (α-BTX) staining of post-synaptic acetylcholine receptors on E18 muscle tissue. Large regions of 1KO;2$^{-/\Delta ILO}$ muscle (white dashed line) lack motor axon innervation. Scale bar, 50μm. (G) Neuromuscular apposition of synaptophysin/NF and α-BTX in limb muscles at E18. SEM, one-way ANOVA, Holm-Sidak multiple comparison test. (H) 1KO;2$^{-/\Delta ILO}$ mice (right) die after E18 cesarean section due to lack of respiration.

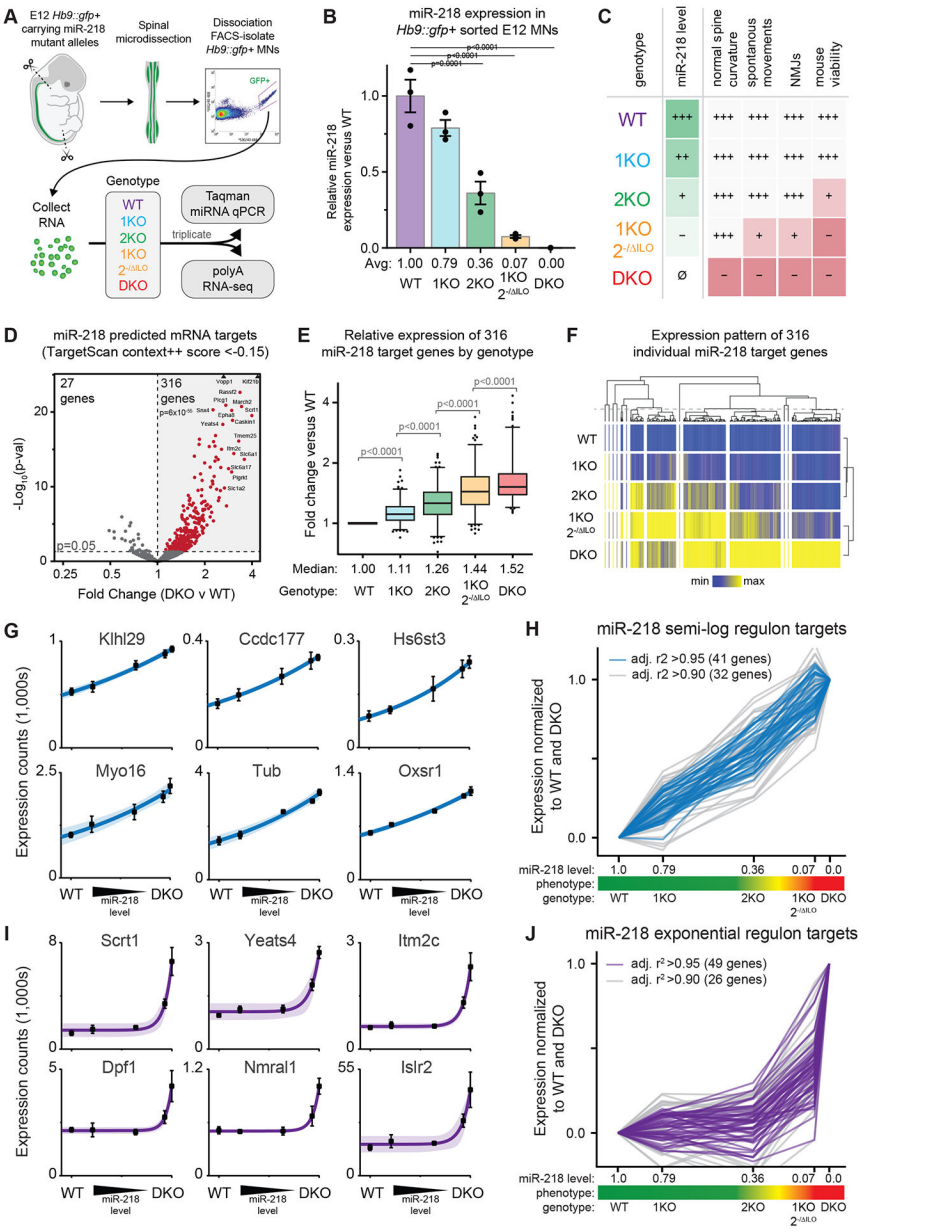

Figure 3.

Wide variance in miR-218 target gene dose responses. (A) *Hb9::gfp+* motor neurons from each respective genotype were FACS-isolated from microdissected embryonic spinal cords in triplicate. (B) miR-218 expression normalized against U6 and the pan-neuronal miR-124 by Taqman qPCR. SEM, one-way ANOVA, Sidak multiple comparison test. (C) miR-218 expression level inversely correlates with phenotypic severity. (D) Identification of 316 high confidence mRNA targets in motor neurons. (E) As a group, miR-218 target mRNAs exhibit stepwise de-repression with decreasing miR-218 expression across genotypes (Repeated measures ANOVA, Holm-Sidak's multiple comparisons test). (F) Hierarchical clustering of target mRNA expression by genotype reveals differences in miR-218 dose responses (Pearson correlation). (G-J) Semi-log and exponential regulons have distinct miR-218 dose-

responses. (G) Representative semi-log and (I) exponential regulon target mRNAs (semi-log and exponential regressions with 95% CI, SEM). Double normalized dose-response curves of (H) semi-log and (J) exponential regulon target mRNAs versus miR-218 level, phenotype, and genotype.

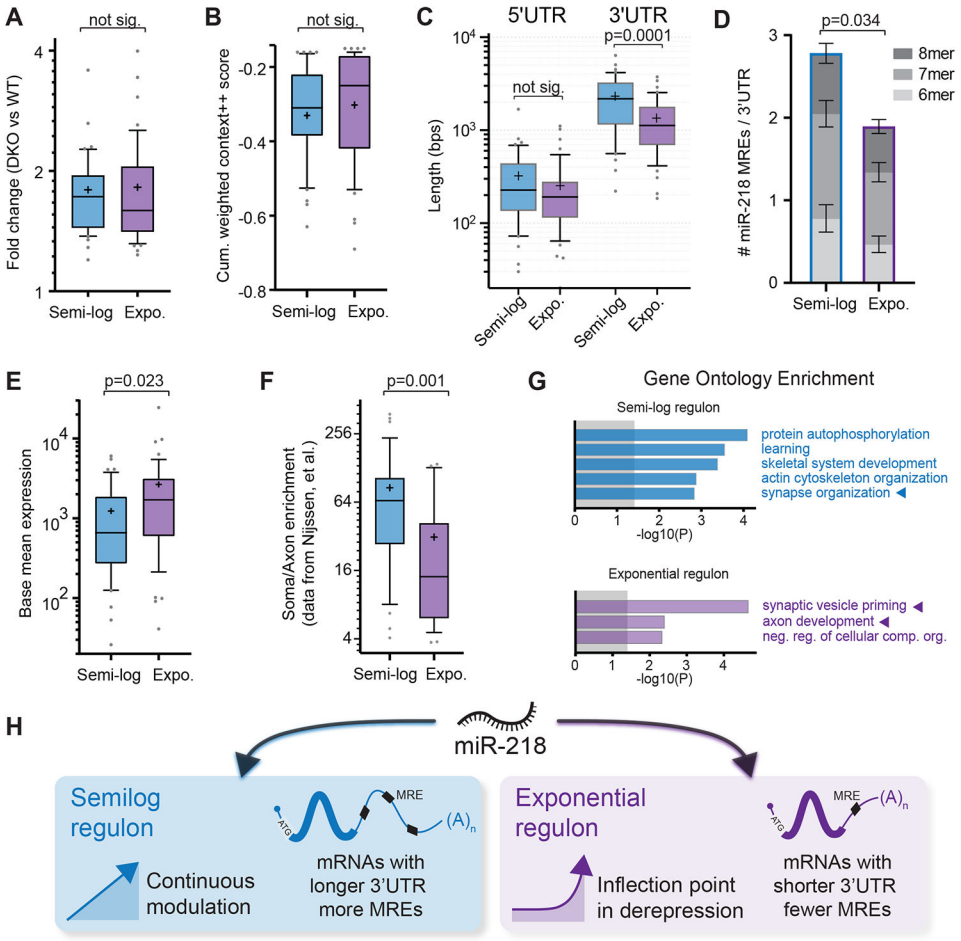

Figure 4.

miR-218 dose responsive regulons are distinguished by 3'UTR characteristics. (A) Magnitude of fold change and (B) bioinformatic prediction of miR-218 targeting efficiency are not significantly different in semi-log and exponential regulons. (C) Semi-log regulon mRNAs have longer 3'UTRs and (D) carry more miR-218 miRNA response elements (MREs) than exponential regulon mRNAs. (E) Exponential regulon mRNAs have higher abundance and (F) are more biased towards the axonal compartment than semi-log regulon mRNAs. (G) GO term enrichment of semi-log and exponential regulons. (H) miR-218 dose proportionally modulates the expression of semi-log regulon mRNAs, which are characterized by longer 3'UTRs and more MREs per mRNA. Exponential regulon mRNAs are highly sensitive to miR-218 dose at low expression levels and their repression is saturated at high levels, resulting in a miR-218 dose-dependent inflection point in target gene de-repression. Mann-Whitney test, multiple hypothesis testing-adjusted p-values reported (Bonferroni-Holm method).

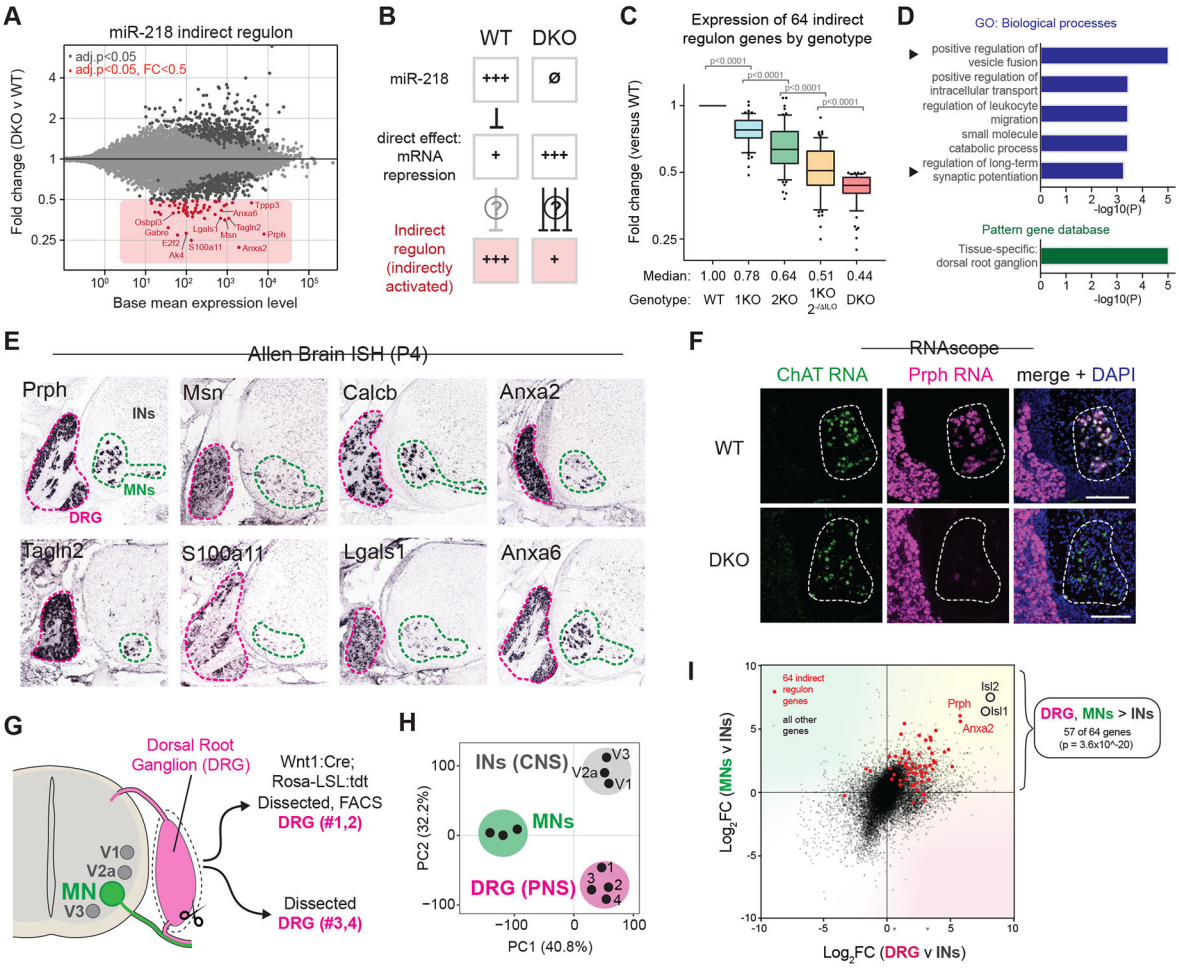

Figure 5.

miR-218 indirectly activates a peripheral neuronal gene signature within motor neurons. (A) 64 mRNAs were significantly de-activated by greater than 50% in DKO motor neurons. (B) These mRNAs, termed the indirect regulon, are indirectly activated by miR-218, potentially as a consequence of direct miR-218-mediated repression of unknown transcriptional repressors or downstream gene network effects. (C) Indirect regulon genes exhibited stepwise de-activation with decreasing miR-218 levels across genotypes. (D) The indirect regulon is associated with synaptic and vesicular processes and a gene signature of dorsal root ganglion (DRG) peripheral sensory neurons. (E) Representative images of the spatial expression pattern of indirect regulon mRNAs in the Allen Brain database in P4 mice. Strong and specific signal is seen in the DRG (magenta) and spinal motor neurons (MNs, green) but not spinal interneurons or glia. Image credit: Allen Institute. (F) Prph RNA is reduced in DKO motor neurons but unchanged in DRG. Scale bar 150μm. (G) We dissected DRG and performed FACS of Wnt1:Cre; Rosa:LSL:tdt embryos in duplicate prior to RNA sequencing. (H) PCA demonstrates separation of spinal MNs, spinal interneurons (INs), and neural crest-derived DRG reflecting their highly distinct transcriptomic identities. In contrast, individual V1, V2a and V3 interneuron subtypes cluster together. (I) Fold-change versus fold-change plot of cellular mRNA enrichment. Indirect regulon genes are enriched

in the top right quadrant, representing higher expression in both DRG and MNs versus interneurons.

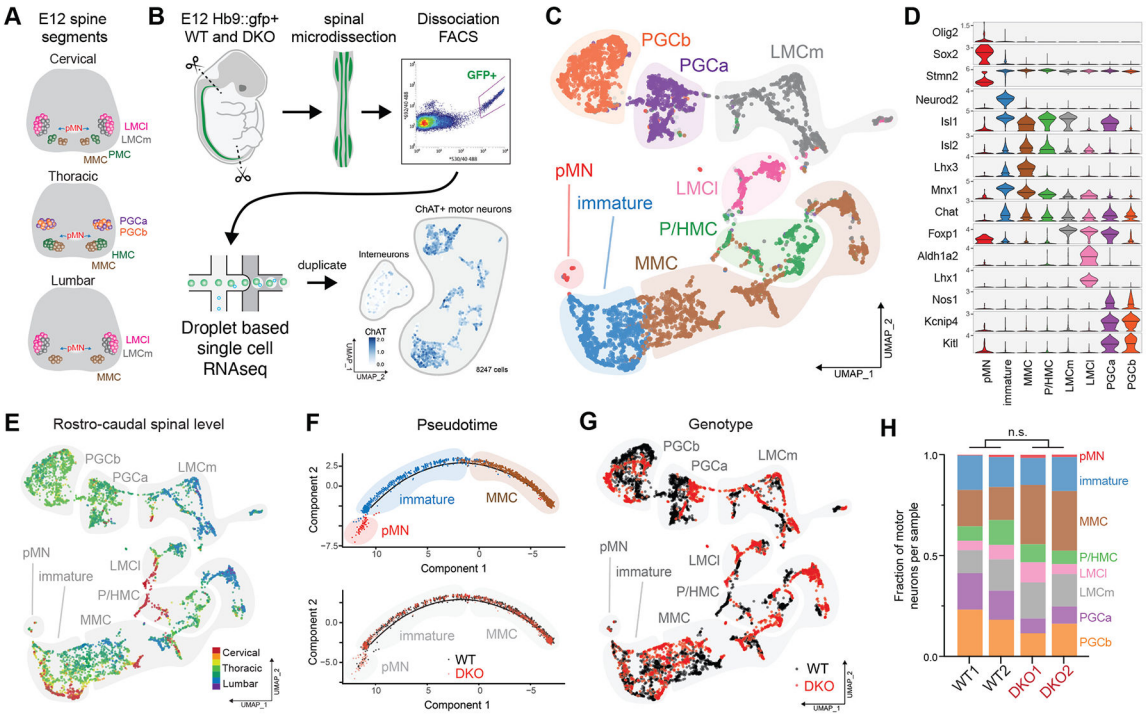

Figure 6.

Motor neuron subtype identity acquisition is not affected by miR-218. (A) Motor neuron spinal diversity along the rostro-caudal axis by motor columns and divisions. (B) Droplet-based scRNA sequencing of FACS-isolated *Hb9::gfp+* motor neurons from microdissected WT and DKO spinal cords. Motor neurons were identified by choline acetyltransferase (ChAT) expression. (C) Guided identification of motor neuron subtypes via (D) expression patterns of known transcription factor markers. (E) Rostro-caudal identity by Hox gene expression. (F) Pseudo-time plot of pMN, immature and MMC motor neurons aligns cells along a neurodevelopmental differentiation timeline and does not segregate by presence or absence of miR-218. (G) UMAP does not segregate motor neurons by genotype. (H) Subtype identity is not significantly affected by the presence or absence of miR-218. pMN, motor neuron progenitors; MMC, medial motor column; P/HMC, phrenic and hypaxial motor column; LMC, lateral motor column – (l) lateral and (m) medial divisions; PGCa/b, preganglionic motor column – (a/b) divisions.

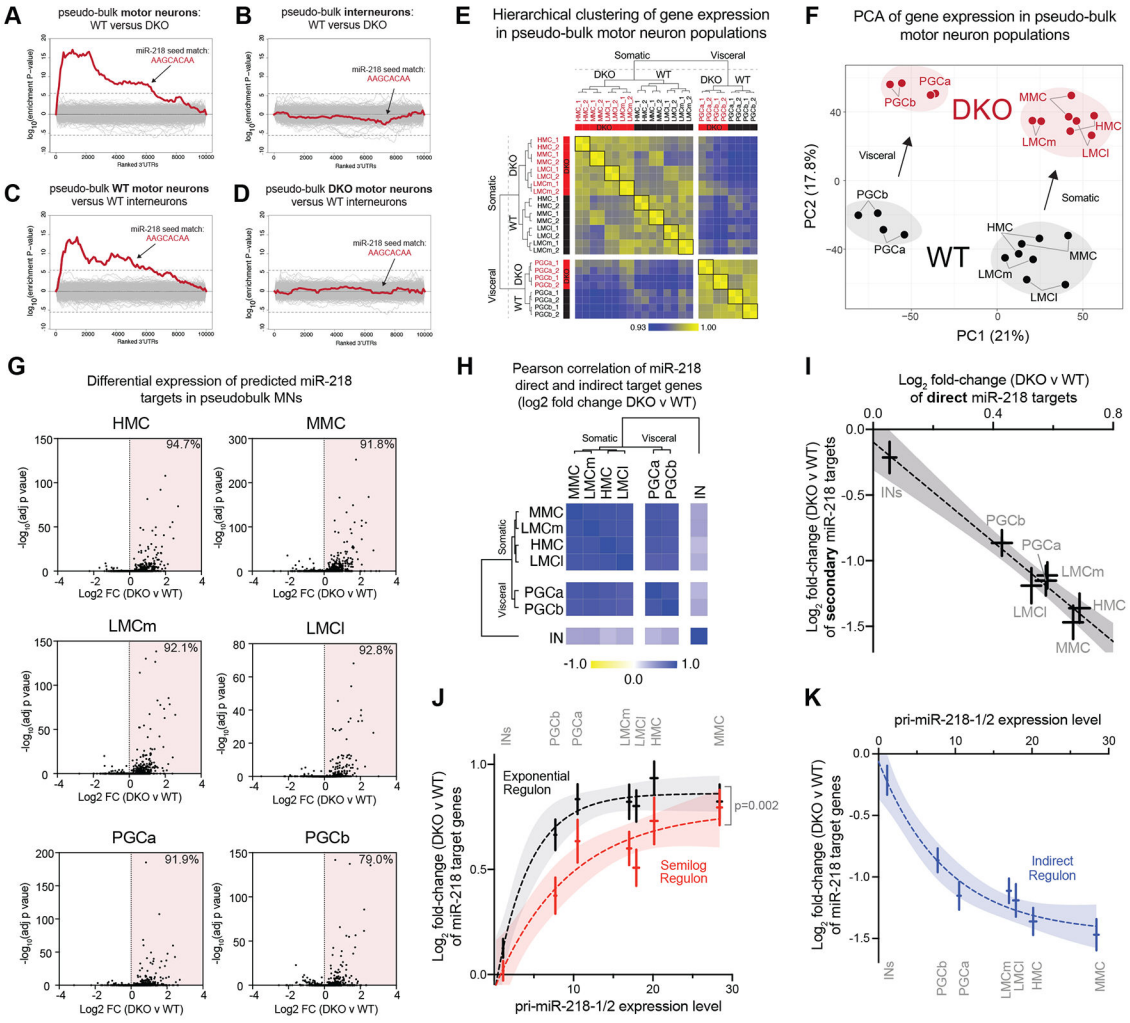

Figure 7.

miR-218 dose-dependent effects differ in magnitude across somatic and visceral motor neuron subtypes. (A-D) Hypergeometric enrichment analysis of 8bp 3'UTR miRNA binding site motifs in ranked gene lists. (A) miR-218's seed sequence (AAGCACAA) is enriched in genes expressed higher in DKO versus WT motor neurons (B) but not DKO versus WT interneurons. (C) miR-218's seed sequence is enriched in genes expressed higher in WT interneurons versus WT motor neurons (D) but not versus DKO motor neurons. (E) Motor neurons of the same genotype, subtype, and replicate were combined *in silico* into individual pseudo-bulk samples. Hierarchical clustering identified divisions in somatic versus visceral motor neurons and further divisions between WT and DKO motor neurons (Pearson correlation). (F) PCA identifies divisions between visceral and somatic motor neurons along PC1 and genotype along PC2. (G) Differential expression of bioinformatically predicted miR-218 targets identifies significant de-repression of targets in DKO versus WT motor neurons within a given subtype. (H) miR-218-mediated effects are highly correlated in motor neuron subtype. (I) Fold-change versus fold-change plot (DKO versus WT) of direct and indirect miR-218 targets by subtype. (J and K) Fold-change (DKO versus WT) of mRNAs within (J) exponential and semi-log and (K) indirect regulons versus

pri-miR-218-1/2 expression level, by motor subtype (error bars: SEM; exponential and indirect regulons: one-phase association regression; semi-log regulon: semi-log regression; 95% CI).

KEY RESOURCES TABLE

REAGENT or RESOURCE	SOURCE	IDENTIFIER
Antibodies		
Neurofilament M	Chemicon	AB1987
Synaptophysin	Santa Cruz	Sc-9116
Alpha-bungarotoxin	Life Technologies	T-1175
Biological Samples		
Adult human spinal cord fresh frozen tissue (61yo male)	John Ravits (UCSD)	N/A
Chemicals, Peptides, and Recombinant Proteins		
LIF	Sigma Aldrich (Calbiochem)	LIF2050
SAG	Sigma Aldrich (Calbiochem)	364590-63-6
Retinoic acid	Sigma Aldrich (Calbiochem)	302-79-4
Critical Commercial Assays		
Papain Dissociation Kit	Worthington Biochemical	Cat# LK003153
T7 Quick High Yield RNA Synthesis Kit	New England Biolabs	Cat# E2050S
mMachine T7 ULTRA Kit	Life Technologies	Cat# AM1345M
Trizol-LS	ThermoFisher	Cat# 10296010
TruSeq RNA Library Preparation Kit	Illumina	V2
Lipofectamine 2000	Invitrogen	Cat# 11668027
Proteinase K	New England Biolabs	Cat# P8107S
Single cell RNA sequencing	10x Genomics	V2
RNAscope Fluorescent Multiplex Assay v1	Advanced Cell Diagnostics, Inc.	Cat# 320850
Taqman Universal Master Mix II	Life Technologies	Cat# 4440040
Deposited Data		
Bulk RNA seq - E12 Hb9:gfp	(this paper)	E12_WT (A-C)
Bulk RNA seq - E12 Hb9:gfp;miR218-1−/−	(this paper)	E12_1KO (A-C)
Bulk RNA seq - E12 Hb9:gfp;miR218-2−/−	(this paper)	E12_2KO (A-C)
Bulk RNA seq - E12 Hb9:gfp;miR218-1−/−;miR218-2-/d-ILO	(this paper)	E12_1KO;2-/d-ILO (A-C)
Bulk RNA seq - E12 Hb9:gfp;miR218-1−/−;miR218-2−/−	(this paper)	E12_DKO (A-C
Bulk RNA seq - mESC Hb9:gfp	(this paper)	ESMN_WT
Bulk RNA seq - mESC Hb9:gfp;CRISPR deletion	(this paper)	ESMN_del_(A-F)
Bulk RNA seq - E12 dissected DRG	(this paper)	DRG (1,2)
Bulk RNA seq - E12 Wnt1:Cre;LSL:tdt; FACS	(this paper)	DRG (3,4)
scRNAseq - E12 Hb9:gfp	(this paper)	MNscWT(1,2)
scRNAseq - E12 Hb9:gfp;miR218-1−/−;miR218-2−/−	(this paper)	MNscDKO(1,2)
Experimental Models: Cell Lines		
Mouse embryonic stem cell line Hb9:gfp+	(Lee et al., 2004)	N/A
Mouse embryonic stem cell line Hb9:gfp+, CRISPR-modified (A-F)	This paper	N/A
Experimental Models: Organisms/Strains		

REAGENT or RESOURCE	SOURCE	IDENTIFIER
Mus musculus		
Rosa-LSL-tdtomato	The Jackson Laboratory	Ai9
Wnt1:Cre	The Jackson Laboratory	E2f1 (Tg(Wnt1-cre)2Sor
Hb9::gfp allele	(Lee et al., 2004)	N/A
miR-218-1 KO (1KO) allele	(Amin et al., 2015)	N/A
miR-218-2 KO (2KO) allele	(Amin et al., 2015)	N/A
miR-218-2-delta-ILO KO allele	This paper	N/A
Mouse: ILOp (908bp) :: eGFP-218-2	This paper	N/A
Oligonucleotides		
miR-218 LNA probe, DIG labelled	Exiqon	Cat# 18111-15
miR-124 LNA probe, DIG labelled	Exiqon	Cat# 88066-15
miR-218 (TaqMan™ MicroRNA Assays)	Thermo Fisher Scientific	Cat# 4427975-000521
miR-124 (TaqMan™ MicroRNA Assays)	Thermo Fisher Scientific	Cat# 4427975-000446
U6 snRNA (TaqMan™ MicroRNA Assays)	Thermo Fisher Scientific	Cat# 4427975-001973
RNAscope® Probe- Mm-Prph-C2	RNAscope	Cat# 400361-C2
RNAscope® Probe- Mm-Chat	RNAscope	Cat# 408731
Recombinant DNA		
ILOp (908bp) :: GFP-pre-mir-218	This paper	N/A
Software and Algorithms		
GraphPad Prism	GraphPad Software	8.2.0
Metascape	(Zhou et al., 2019)	N/A
Adobe Illustrator	Adobe	23.1.1
CRISPR design tool	Zhang Lab MIT	N/A
RStudio	www.rstudio.com	1.2.1335
Galaxy	(Afgan et al., 2018)	0.43.1.3
UCSC genome browser	https://genome.ucsc.edu	N/A
Integrated Genomics Viewer (IGV)	Broad Institute	N/A
Sylamer	(van Dongen et al., 2008)	N/A
Morpheus	Broad Institute	N/A
ClustVis	(Metsalu and Vilo, 2015)	N/A
ImageJ	National Institutes of Health	N/A